Biomedicine & Pharmacotherapy 171 (2024) 116127

Contents lists available at ScienceDirect

Biomedicine & Pharmacotherapy

journal homepage: www.elsevier.com/locate/biopha

Role of the soluble epoxide hydrolase in keratinocyte proliferation and sensitivity of skin to inflammatory stimuli

Zumer Naeem [a], Sven Zukunft [a], Arnaud Huard [b,1], Jiong Hu [a,c], Bruce D. Hammock [d], Andreas Weigert [b], Timo Frömel [a], Ingrid Fleming [a,e,f,*]

[a] Institute for Vascular Signalling, Centre for Molecular Medicine, Goethe University, Frankfurt am Main, Germany
[b] Institute of Biochemistry I, Goethe-University Frankfurt, Frankfurt am Main 60590, Germany
[c] Department of Embryology and Histology, School of Basic Medicine, Tongi Medical College, Huazhong University of Science and Technology, Wuhan, China
[d] Department of Entomology and Nematology and Comprehensive Cancer Center, University of California, Davis, CA, USA
[e] German Center of Cardiovascular Research (DZHK), Partner site RheinMain, Frankfurt am Main, Germany
[f] CardioPulmonary Institute, Goethe University, Frankfurt am Main, Germany

ARTICLE INFO

Keywords:
Dermatitis
Polyunsaturated fatty acid mediators
Psoriasis
Soluble epoxide hydrolase

ABSTRACT

The lipid content of skin plays a determinant role in its barrier function with a particularly important role attributed to linoleic acid and its derivatives. Here we explored the consequences of interfering with the soluble epoxide hydrolase (sEH) on skin homeostasis. sEH; which converts fatty acid epoxides generated by cytochrome P450 enzymes to their corresponding diols, was largely restricted to the epidermis which was enriched in sEH-generated diols. Global deletion of the sEH increased levels of epoxides, including the linoleic acid-derived epoxide; 12,13-epoxyoctadecenoic acid (12,13-EpOME), and increased basal keratinocyte proliferation. sEH deletion ($sEH^{-/-}$ mice) resulted in thicker differentiated spinous and corneocyte layers compared to wild-type mice, a hyperkeratosis phenotype that was reproduced in wild-type mice treated with a sEH inhibitor. sEH deletion made the skin sensitive to inflammation and $sEH^{-/-}$ mice developed thicker imiquimod-induced psoriasis plaques than the control group and were more prone to inflammation triggered by mechanical stress with pronounced infiltration and activation of neutrophils as well as vascular leak and increased 12,13-EpOME and leukotriene (LT) B4 levels. Topical treatment of LTB4 antagonist after stripping successfully inhibited inflammation and neutrophil infiltration both in wild type and $sEH^{-/-}$ skin. While 12,13-EpoME had no effect on the trans-endothelial migration of neutrophils, like LTB4, it effectively induced neutrophil adhesion and activation. These observations indicate that while the increased accumulation of neutrophils in sEH-deficient skin could be attributed to the increase in LTB4 levels, both 12,13-EpOME and LTB4 contribute to neutrophil activation. Our observations identify a protective role of the sEH in the skin and should be taken into account when designing future clinical trials with sEH inhibitors.

1. Introduction

Omega-3 and ω-6 polyunsaturated fatty acids (PUFAs) have been attributed beneficial effects in various chronic inflammatory and autoimmune diseases. Most of the positive effects of these lipids are unlikely to be direct but rather attributable to their metabolism to bioactive mediators by enzymes such as the cyclooxygenases, lipoxygenases (LOXs) and cytochrome P450 (CYP) enzymes. For example, the substrate arachidonic acid can be metabolized by COX enzymes to give prostaglandins (PGs) and thromboxane, by LOX enzymes to give leukotrienes (LTs) and by CYP enzymes to generate epoxyeicosatrienoic acids (EETs) and hydroxy metabolites such as 20-hydroxyeicosatetraenoic acid (20-HETE) (for review see [1]). The CYP enzymes are the least well studied of the three enzyme families but are probably the most versatile as they can accept several different ω-6 and ω-3 PUFAs as substrates to generate an impressive array of PUFA epoxides with biological activity [2]. Interest in the PUFA epoxides was triggered by the realization that many of these mediators exhibit vasodilator [3,4] and anti-inflammatory properties [5], but the biological actions of these mediators is now known to be much broader [6,7].

* Correspondence to: Institute for Vascular Signalling, Centre for Molecular Medicine, Goethe University, Theodor Stern Kai 7, 60596 Frankfurt am Main, Germany.
E-mail address: fleming@em.uni-frankfurt.de (I. Fleming).
[1] Current address: Department of Pathology and Immunology, Faculty of Medicine, University of Geneva, 1211 Geneva, Switzerland

https://doi.org/10.1016/j.biopha.2024.116127
Received 4 November 2023; Received in revised form 31 December 2023; Accepted 2 January 2024
Available online 9 January 2024

In cells and tissues, the biological half-life of the CYP–derived PUFA epoxides is determined by their hydroxylation to diols, largely by the soluble epoxide hydrolase (sEH; gene name *Ephx2*). The enzyme is a homodimer and is highly expressed in many tissues, including the liver, kidney, brain and heart. Intriguingly, the sEH has two active domains; the C-terminal domain possesses epoxide hydrolase activity and adds water to fatty acid epoxides, thus generating their respective diols. The PUFA diols are generally thought to be less active, or even inactive, compared to the corresponding epoxides, and are certainly more polar, easily conjugated and excreted (for reviews see references [1,8]). The N-terminal domain of the sEH is thought to be a lipid phosphatase [9, 10], that is able to dephosphorylate substrates such as farnesyl and geranylgeranyl pyrophosphate as well as sphingosine-1-phosphate and lysophosphatidic acid, at least in vitro (for review see [11]). A physiological role for the lipid phosphatase activity of the sEH remains to be demonstrated but there is a mountain of evidence linking low epoxide

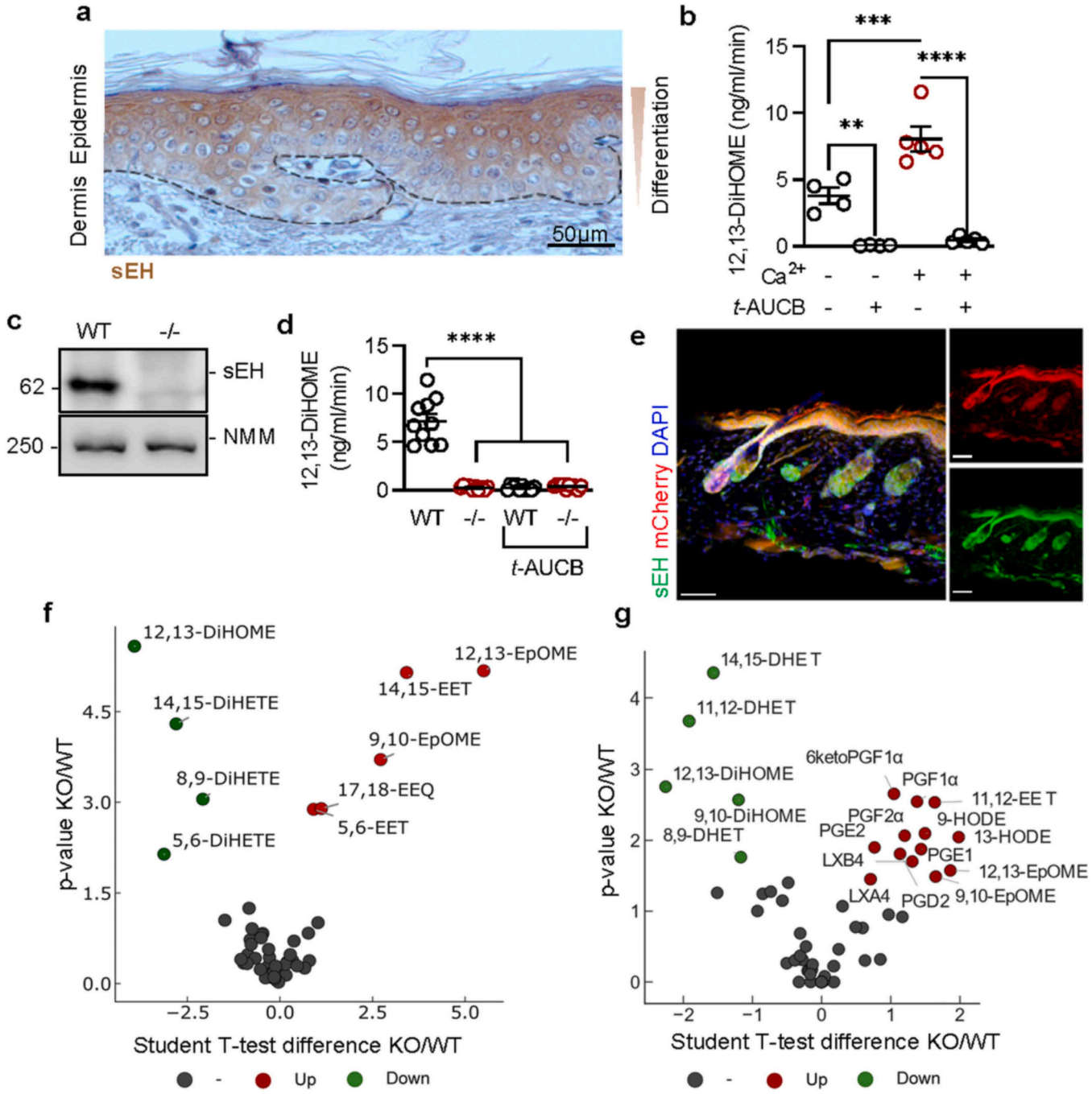

Fig. 1. sEH expression and activity in human and murine skin. (**a**) sEH expression in human skin. The results shown are representative of findings obtained in 4 additional preparations, all from different donors. (**b**) sEH activity in undifferentiated and Ca^{2+}-differentiated human keratinocytes in the absence and presence of the sEH inhibitor *t*-AUCB; n = 2 independent experiments (one way ANOVA and Tukey's multiple comparison test). (**c**) sEH protein expression in dorsal skin from wild-type (WT) and $sEH^{-/-}$ (-/-) mice. The blots shown are representative of data obtained in 5 additional animals per group. (**d**) sEH activity in dorsal skin from wild-type (WT) and $sEH^{-/-}$ (-/-) mice. Experiments were performed in the absence and presence of *t*-AUCB; n = 10 mice per group (two way ANOVA and Tukey's multiple comparison test). (**e**) sEH expression in the skin of a sEH-tdTomato reporter mouse. Note that the endogenous Tomato signal was amplified with an mCherry antibody; bar = 50 µm. (**f&g**) Volcano plots showing the most altered PUFA metabolites in dorsal skin from wild-type (WT) versus $sEH^{-/-}$ (KO) mice during the resting phase (f), and the hair growth phase (g); n = 5–8 animals per group. * *P < 0.01, * **P < 0.001, * ** *P < 0.0001.

hydrolase activity to physiology [7,12]. Targeting the sEH in animal models using genetic interventions or pharmacological inhibitors effectively increases tissue and circulating levels of the epoxides and has helped elucidate the role of PUFA mediators in modulating inflammation linked with cardiovascular pathology, inflammatory pain, neuro-inflammation and metabolic disorders [13–17]. The over-expression of the sEH, on the other hand, tends to be associated with pathophysiology such as hypertension [18–20], and vascular instability

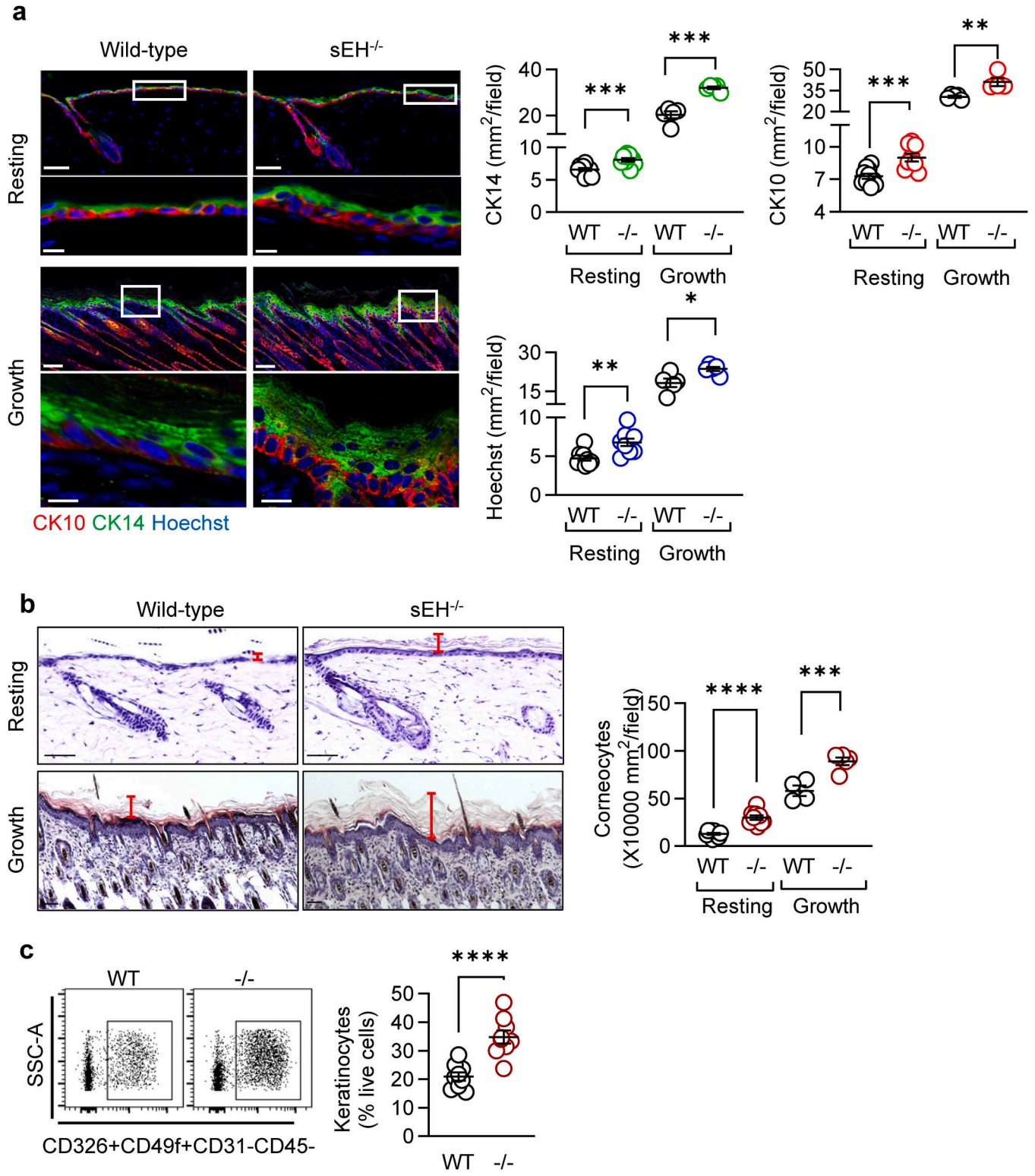

Fig. 2. Consequences of sEH deletion on the epidermal stratification and terminal differentiation. (**a**) Cytokeratin (CK) 14, CK10 and Hoechst staining in the skin from wild-type (WT) and sEH$^{-/-}$ (-/-) mice during the resting (a) and growth (b) phases of the hair follicle cycle, bar = 50 μm. The lower panels show a higher magnification of the area marked by white boxes. Bar = 10 μm; n = 5–8 mice per group (Student's t test). (**b**) Hematoxyline and eosine staining of skin from the same animals as in (a) to highlight the corneocyte scales (red bars), bar = 50 μm; n = 5–8 mice per group (Student's t test). (**c**) FACS analysis of epidermal keratinocytes in skin from wild-type (WT) and sEH$^{-/-}$ (-/-) mice; n = 9 animals per group (Student's t test). *P < 0.05, * *P < 0.01, * **P < 0.001, * ** *P < 0.0001.

[21,22].

Even though CYP enzymes and epoxide hydrolases have been detected in human and murine skin [23–25], almost nothing is known about their physiological/pathophysiological role in barrier function or repair. More information about the role of CYP and sEH-derived metabolites in skin function is needed, particularly given the fact that in a recent first-in-human study using the sEH inhibitor GSK2256294, one reported adverse effect of the compound was contact dermatitis [26]. The aim of this study was, therefore, to investigate the impact of sEH deletion/inhibition on the dermal eicosanoid profile, and assess the consequences of altered sEH activity on skin inflammation.

2. Results

2.1. Influence of sEH deletion on PUFA mediator levels in skin

Immuno-staining of human skin revealed that sEH was expressed in the epidermis and that its expression increased gradually with increased cell differentiation in the stratified layers (Fig. 1**a**). In agreement with this, sEH activity in cultured human keratinocytes was significantly increased following Ca^{2+}-induced differentiation and was sensitive to the sEH inhibitor, *t*-AUCB (Fig. 1**b**). Consistent with these findings, sEH was expressed (Fig. 1**c**), and active (Fig. 1**d**) in skin from wild-type but not $sEH^{-/-}$ mice. In skin from a novel sEH-tdTomato reporter mouse, the enzyme was detected in the epidermis as well as in epidermal cells lining the hair follicle (Fig. 1**e**, Supplementary Fig. 1).

Given the role of the sEH in PUFA metabolism, we next compared levels of PUFA-derived mediators in the epidermal and dermal layers of murine skin. Similar to the situation reported for human skin [27], PUFA metabolites generated by COX and LOX enzymes were more abundant in the epidermis than in the dermis. CYP-derived oxylipins were comparable in both layers but, fitting with the localization of the enzyme, sEH-generated diols were enriched in the epidermis (Supplementary Fig. 2). A comparison of dorsal skin from wild-type and $sEH^{-/-}$ mice revealed that the deletion of the sEH resulted in an increase in PUFA epoxides including; 5,6- and 14,15-EET, 17,18-epoxyeicosatetraenoic acid (EEQ), as well as 9,10- and 12,13-epoxyoctadecenoic acid (12, 13-EpOME). There was also a significant decrease in PUFA diols i.e., 5, 6-, 8,9-, and 14,15-dihydroxyeicosatrienoic acid (DHET), as well as 12, 13-dihydroxyoctadecenoic acid (DiHOME) (Fig. 1**f**). The differences in CYP/sEH-derived metabolites between wild-type and $sEH^{-/-}$ mice were consistent in skin obtained during the resting and growth phases of the hair follicle cycle (i.e. 7 - 8 week old versus 32-day old mice). However, during the hair growth phase sEH deletion also significantly affected the levels of PGs including PGE_1, PGE_2, PGD_2, $PGF_{1\alpha}$ and $PGF_{2\alpha}$, as well as the oxidized linoleic acid derivatives 9- and 13-hydroxyoctadecadienoic acid (HODE) (Fig. 1**g**).

2.2. Consequences of sEH deletion and inhibition on keratinocytes

Some of the metabolites elevated in skin from $sEH^{-/-}$ mice i.e. 11,12- and 14,15-EET as well as 13(S)-HODE, have been implicated in keratinocyte differentiation in ex vivo systems [28–30]. Therefore, epidermal stratification and terminal differentiation were assessed. Skin from $sEH^{-/-}$ mice contained more cytokeratin (CK) 14 + basal keratinocytes, and CK10 + spinous keratinocytes than skin from wild-type mice during the resting and growth stages of the follicle cycle (Fig. 2**a**). Also, more corneocyte scales were apparent on the surface of the skin from $sEH^{-/-}$ than wild-type mice (Fig. 2**b**). Flow cytometry revealed a significant increase in keratinocyte numbers ($CD326^+CD49f^+CD31^-CD45^-$ cells) in sEH-deficient skin (Fig. 2**c**). In the same samples there was no difference in the numbers of immune cells (CD45 +) but a significant decrease in fibroblasts (CD45-CD49f+CD90.2 +) as well as lymphatic endothelial cells (CD45-CD49f+CD31 +CD90.2 +CD326-) in sEH-deficient skin (Supplementary Fig. 3). These findings implicate the sEH in processes involved in keratinocyte proliferation and skin stratification.

The sEH is a bifunctional enzyme and while its C-terminus possesses epoxide hydrolase activity, the N-terminal domain is reported to be a lipid phosphatase [9,10]. Therefore, to confirm the role of an epoxide hydrolase on keratinocyte homeostasis, the sEH inhibitor TTPU, was applied topically to the shaven skin of wild-type animals. The application of TPPU over 4 days altered the PUFA metabolite profile in murine skin (Fig. 3**a**), and increased the epidermal thickness as assessed by the number of nuclei (Hoechst staining) present in the epidermis (Fig. 3**b**). sEH inhibition also increased the numbers of CK14 + as well as CK10 + cells. The expression of involucrin, a cornified envelope protein expressed by keratinocytes in the stratum corneum early in their terminal differentiation [31], was also increased by TPPU treatment (Fig. 3**c**).

2.3. Comparison of imiquimod-induced psoriasis in wild-type and $sEH^{-/-}$ mice

Since the deletion and inhibition of the sEH affected keratinocyte proliferation, we assessed its role in psoriasis, a situation resulting from the hyper-proliferation but arrested differentiation of keratinocytes [32, 33]. Immunostaining in human skin revealed that sEH expression was lower in psoriatic lesions than in non-lesional skin from the same subject (Fig. 4**a**). To study the consequences of this change in mice, psoriasis was induced by applying imiquimod to freshly shaven skin for 6 days followed by a period of resolution for an additional 4 days [34]. In wild-type mice the daily application of imiquimod to dorsal skin induced inflamed scaly skin lesions resembling plaque-type psoriasis and was associated with an increase in skin thickness that peaked between days 3 and 6 (Fig. 4**b**). The response was more marked in $sEH^{-/-}$ mice, in which skin thickness reached a maximum during the acute phase (day 3) and skin remained thicker even during resolution (days 6–10). While the vascularization of the skin was not different between the genotypes, fewer lymphatic endothelial cells (lyve1 +) were detected in psoriatic skin from $sEH^{-/-}$ mice on day 3 (Fig. 4**c**), a situation that had resolved by day 6 (Supplementary Fig. 4a). Keratinocyte proliferation (Ki67 staining and an increase in CK14 + cells) was also elevated in $sEH^{-/-}$ mice on day 3 (Fig. 4**d**), but responses were comparable in wild-type and $sEH^{-/-}$ mice on day 6 (Supplementary Fig. 4b**&c**). Even though there were more differentiated CK10 + cells in the spinous layer of sEH-deficient skin under control conditions (see Fig. 3b), fewer CK10 + cells were detected in $sEH^{-/-}$ than wild-type skin after the induction of psoriasis, on both days 3 and 6.

Psoriasis is considered to be an immune-mediated disease in which intra-lesional T lymphocytes and their pro-inflammatory signals trigger basal layer keratinocytes to proliferate [32], but is also associated with the infiltration of neutrophils and macrophages [35]. Interestingly, lesional skin from $sEH^{-/-}$ mice contained significantly fewer αβT cells (CD45 +CD11b-CD3e+) and γδT cells (CD45 +CD11b-CD3e+ γδTCR+) than skin from wild-type mice. FACS-based immune cell profiling of single cell suspensions from dorsal skin revealed that neutrophil (CD45 +CD11b+Ly6G+) and macrophage (CD45 +CD11b+Ly6G-MHC-II+) infiltration into skin was greater in the absence of sEH (Fig. 4**e**). Psoriatic skin frequently contains micro abscess containing neutrophils that migrate to the horny layer of the epidermis [36], and skin from $sEH^{-/-}$ mice demonstrated significantly more micro abscess on days 3 and 6 after imiquimod application than wild-type mice (Fig. 4**d**).

2.4. Consequences of sEH deletion in a model of mechanical injury

As our data suggested that elevated neutrophil recruitment contributed to imiquimod-induced psoriasis in $sEH^{-/-}$ mice, a model of atopic dermatitis linked with mechanical stress-induced inflammation was studied as it is reportedly reliant on neutrophil infiltration [37]. This model of mechanical stress was also felt to be more relevant to the contact dermatitis reported in subjects treated with an sEH inhibitor [26]. Therefore, the dorsal skin of wild-type and $sEH^{-/-}$ mice was

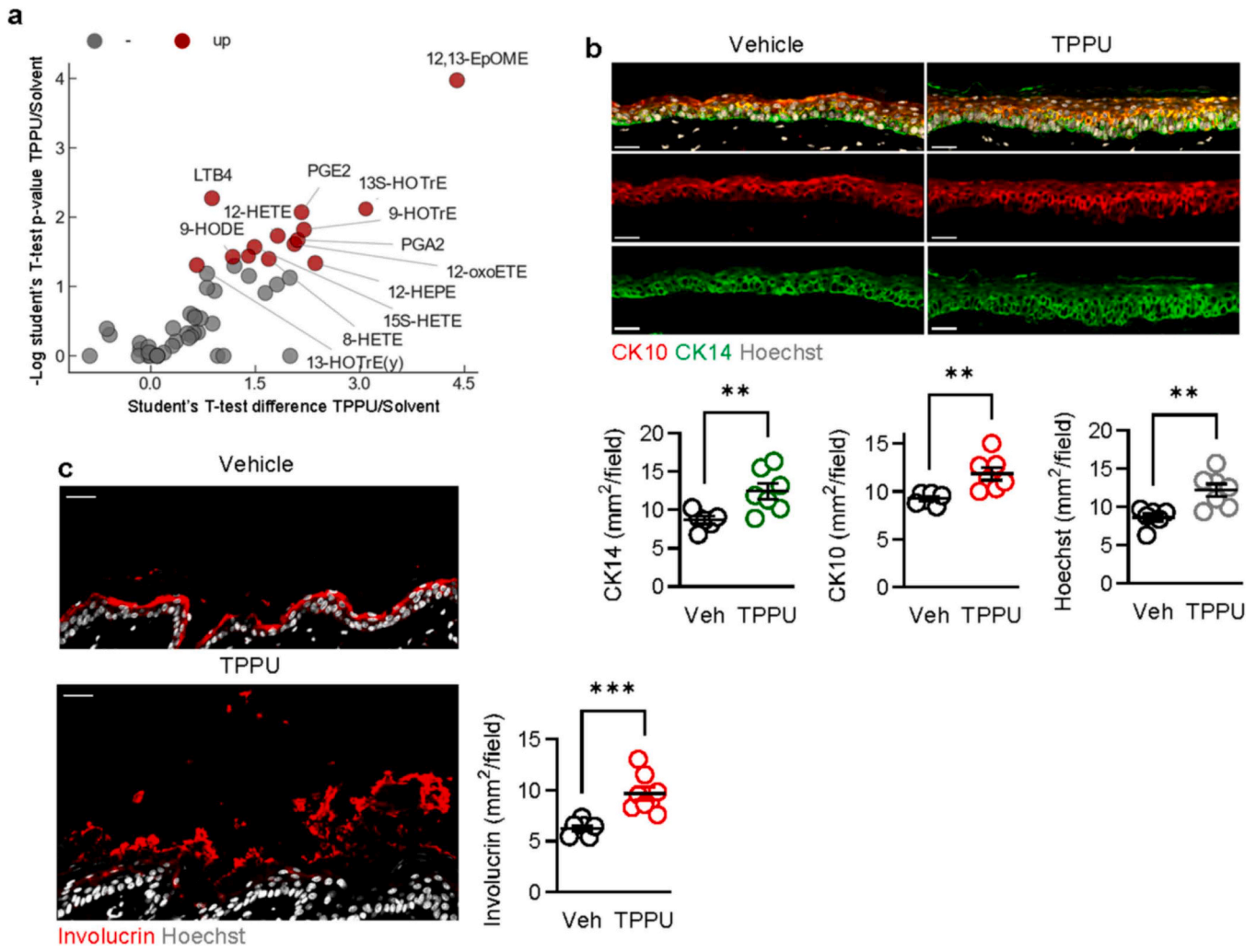

Fig. 3. Consequences of sEH inhibition on PUFA metabolites, the epidermal stratification and hyperkeratosis. (**a**) Volcano plot showing the most altered PUFA metabolites in dorsal skin from wild-type mice treated with vehicle or the sEH inhibitor; TPPU; n = 4 mice per group. (**b**) Cytokeratin (CK)14, and CK10 expression in dorsal skin from wild-type mice after shaving and treatment with vehicle (Veh) or TPPU for 4 days, bar = 30 μm; n = 6–7 mice per group (Student's t test). (**c**) Involucrin staining in dorsal skin from wild-type mice after shaving and treatment with vehicle (Veh) or TPPU for 4 days, bar = 30 μm; n = 6–7 mice per group (Student's t test). * *P < 0.01, * **P < 0.001.

depilated to remove the stratum corneum and render skin vulnerable to inflammation, this process was followed by tape stripping to mimic scratching-induced atopic dermatitis [38,39]. Dorsal skin from sEH$^{-/-}$ mice appeared more irritated after shaving/depilation compared to the skin in wild-type mice (Fig. 5**a**). Subsequent tape stripping induced pronounced skin inflammation and was accompanied by increased perfusion and vascular leakage evidenced by red exudate on the skin surface and more dilated blood vessels on the underside of the skin (Fig. 5**b**). Vascular barrier function was compromised by stripping, as confirmed by studying the leak of Evans blue in dorsal skin (Fig. 5**c**), and was accompanied by neutrophil influx (Fig. 5**d**), all of which were significantly more pronounced in skin from sEH$^{-/-}$ mice. Although more macrophages were detected in the skin of sEH$^{-/-}$ mice after shaving, there were no differences in macrophage numbers in the skin from wild-type and sEH$^{-/-}$ mice following additional mechanical injury (Supplementary Fig. 5). While there were no differences in the numbers of Langerhans cells and αβT cells in the skin from wild-type and sEH$^{-/-}$ mice, sEH deletion was associated with a decrease in γδT cells in stripped skin, as was the case in the psoriasis model.

2.5. *Effect of 12,13-EpOME and LTB4 on neutrophil activation*

To identify a substrate or product of the sEH that could contribute to mechanical stress-induced skin inflammation, PUFA mediator profiling of unshaven versus tape-stripped skin was performed. The most marked effects of mechanical stimulation were on levels of thromboxane B_2, 12-hydroxyheptadeca-5Z,8E,10E-trienoic acid (12-HHT), $PGF_{2\alpha}$, PGE_2 and leukotriene (LT) C4 but comparable changes were detected in wild-type and sEH$^{-/-}$ mice (Fig. 6**a**). Stripped skin from sEH$^{-/-}$ mice contained less 12,13-DiHOME, PGD_2, and EPA but more LTB4, 5-HETE and 12,13-EpOME than stripped skin from wild-type mice (Fig. 6**b**).

Neutrophil recruitment to inflamed, tape-stripped skin has been suggested to be driven by LTB4 [37]. Certainly, the LOX/LTB4/BLT1 axis is important for leukocyte recruitment to sites of inflammation [40]. LTB4 is generated from arachidonic acid through sequential actions of 5-LOX, 5-lipoxygenase-activating protein (FLAP) and the LTA4 hydrolase (LTA4H) [41]. Whereas *Alox5* and *Lta4h* expression were comparable in skin from wild-type and sEH$^{-/-}$ mice, both before shaving and after stripping, the expression of the LTB4 receptor i.e. *Ltb4R* (BLT1), was higher in dorsal skin from sEH$^{-/-}$ than wild-type mice after stripping (Fig. 7**a**). The latter phenomenon most likely reflects the higher recruitment of BLT1-expressing neutrophils to sEH-deficient skin [42].

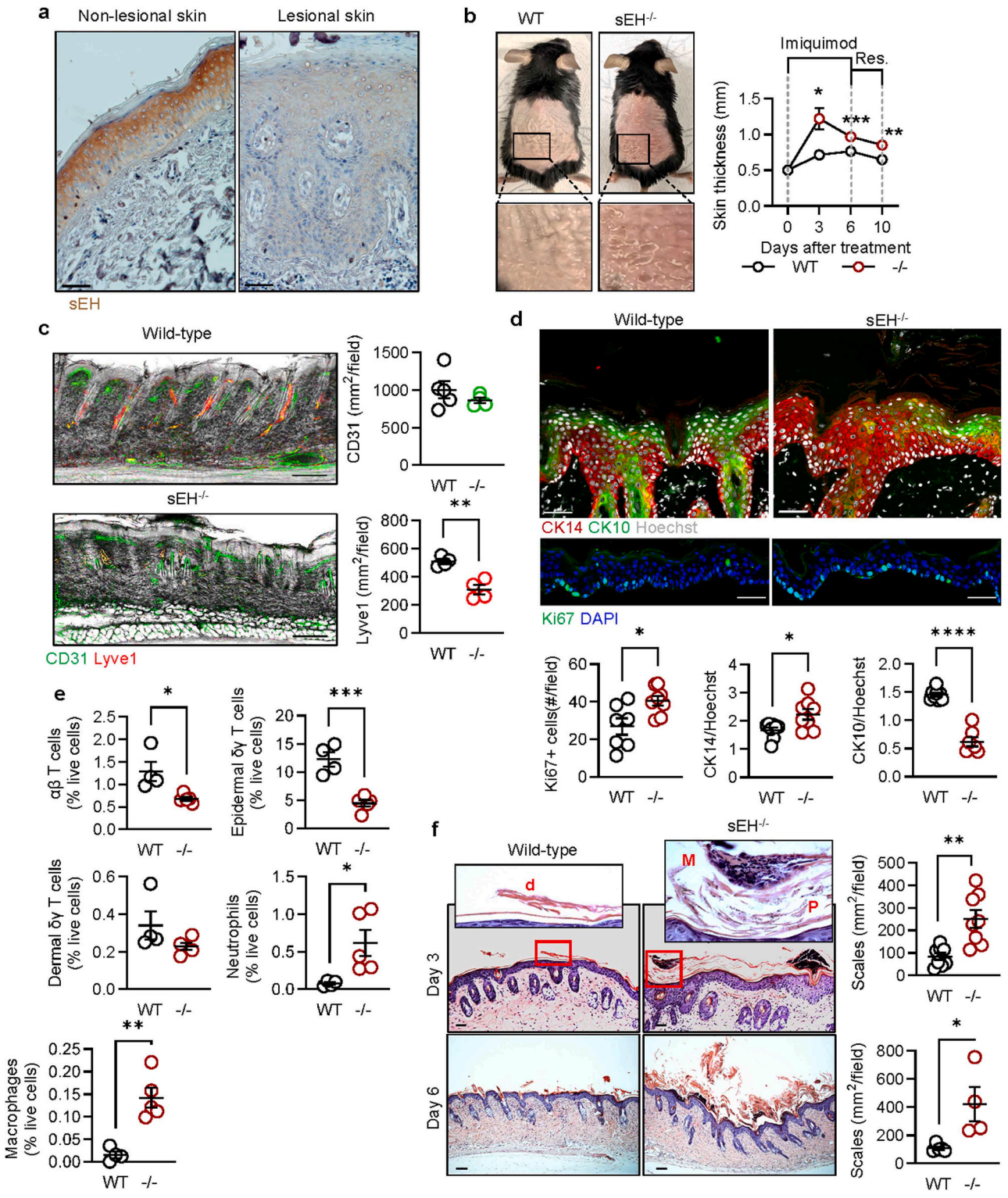

Fig. 4. Comparison of imiquimod-induced inflammation in wild-type and sEH$^{-/-}$ mice. (**a**) sEH expression in lesional (psoriatic) and respective non-lesional human skin. The results shown are representative of findings obtained in 2 additional preparations, all from 4 different donors, size bar = 50 μm. (**b**) Scaly skin lesions resembling plaque type psoriasis (left panels) in wild-type (WT) and sEH$^{-/-}$ (-/-) mice on day 5 and changes in skin thickness (right panel) measured during the application of imiquimod and the 4 day resolution (Res) phase; n = 7–14 mice per group (two way ANOVA and Sidak's multiple comparison test). (**c**) CD31 and Lyve1 in dorsal skin from wild-type (WT) and sEH$^{-/-}$ (-/-) mice, 3 days after treatment with imiquimod, bar = 50 μm; n = 4–5 mice per group (Student's t test). (**d**) CK14, CK10 and Ki67 + cells in dorsal skin from wild-type (WT) and sEH$^{-/-}$ (-/-) mice, 3 days after treatment with imiquimod, bar = 50 μm; n = 5–7 mice per group (Student's t test). (**e**) FACS analysis of immune cells isolated from dorsal skin of wild-type (WT) and sEH$^{-/-}$ (-/-) mice after 3 days of treatment with imiquimod; n = 5–8 animals per group (Student's t test). (**f**) Haematoxylin and eosin staining of psoriatic skin and quantification of scales (inserts) 3 and 6 days after imiquimod treatment, bar = 100 μm; n = 4–9 mice per group (Student's t test). P = parakeratosis, M = microabscess, d = desequamation. *P < 0.05, * *P < 0.01, * **P < 0.001,* ** *P < 0.0001.

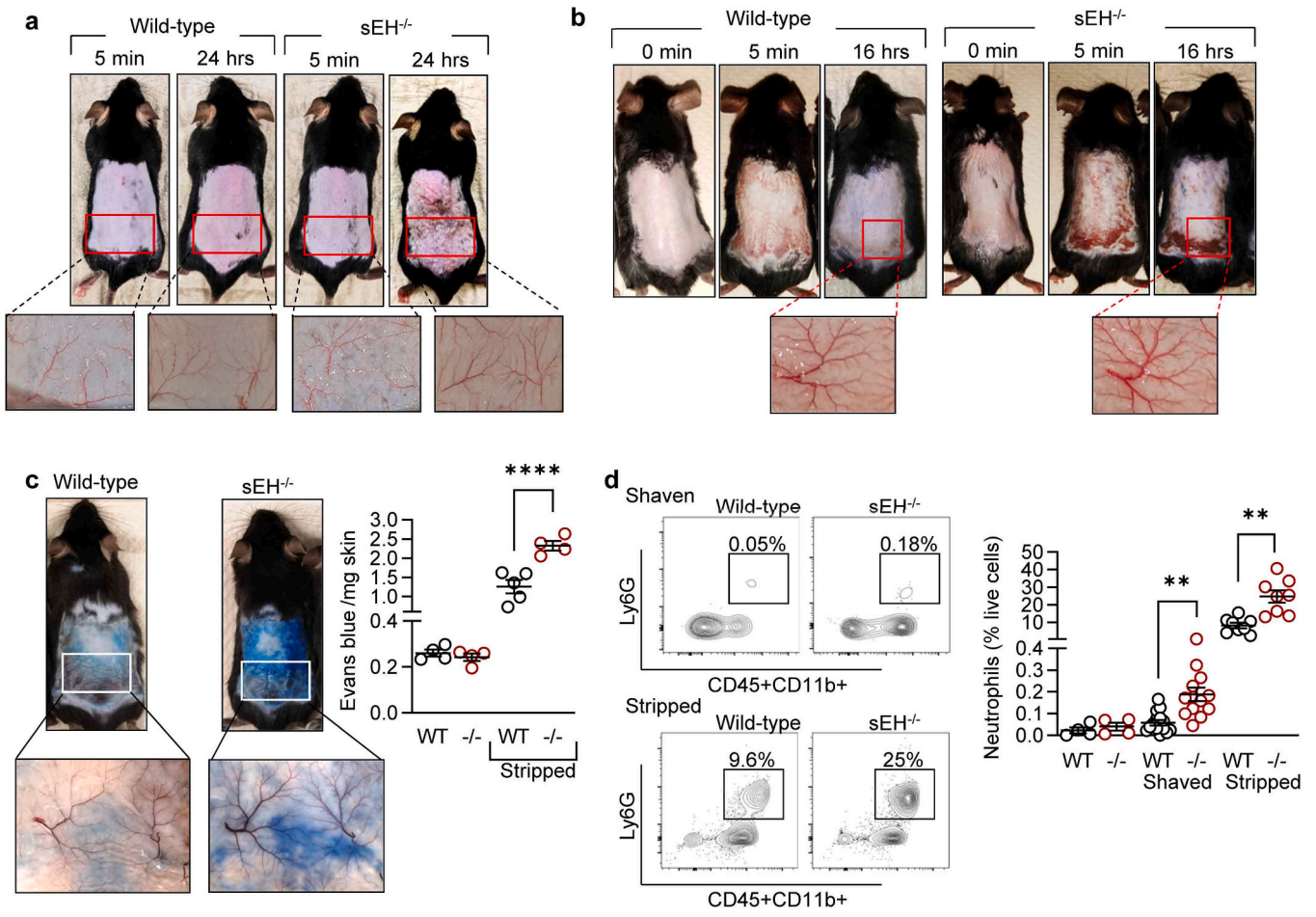

Fig. 5. Consequences of sEH deletion on skin sensitivity to mechanical injury. (**a&b**) Images of dorsal skin from wild-type and sEH$^{-/-}$ animals after shaving (a) or shaving and subsequent repetitive tape stripping (b). Comparable results were obtained in 6 additional animals of each genotype, in 3 independent experiments. The inserts show the underside of the skin in the area marked by red boxes. (**c**) Vascular leak determined by the Evans Blue content of dorsal skin 16 h after stripping. The lower images show the Evans blue accumulation in the underside of the area marked by the white box; n = 4–5 mice per group (two-way ANOVA and Sidak's multiple comparison test). (**d**) Neutrophil content (CD45 +CD11b+Ly6G+) in the skin of unshaven wild-type (WT) and sEH$^{-/-}$ (-/-) mice and 16 h after either shaving or shaving and stripping; n = 4–15 mice per group (two-way ANOVA and Sidak's multiple comparison test). * *P < 0.01, * ** *P < 0.0001.

Indeed, blocking the BLT1 receptor using U-75302 reduced neutrophil infiltration (Fig. 7**b**) as well as the vascular response on the underside of the skin (Fig. 7**c**) to a similar extent in both genotypes. To assess skin barrier function, transepidermal water loss was determined. Water loss was comparable in both genotypes immediately after stripping but lower in stripped skin from sEH$^{-/-}$ mice after 16 h. At first sight this effect seemed to be contradictory but can probably be attributed to the increased vascular leak detected in the sEH deficient mice (see Fig. 5c). Importantly, while U-75302 had no effect on transepidermal water loss, it was clearly decreased by 12,13-EpOME in wild-type mice (Fig. 7**d**). Adding 12,13-EpOME to the sEH$^{-/-}$ mice, which already demonstrated elevated 12,13-EpOME levels, was without additional effect.

To make a direct comparison of the effects of LTB4 and 12,13-EpOME, neutrophil adhesion, activation and endothelial cell trans-migration were assessed. 12,13-EpOME and LTB4 were both effective in inducing neutrophil adhesion to recombinant intracellular adhesion molecule-1 (Fig. 7**e**) as well as in inducing neutrophil activation, as assessed by increased neutrophil elastase activity (Fig. 7**f**). However, when trans-endothelial migration through murine lung endothelial cells was assessed in a Boyden chamber, LTB4 elicited pronounced trans-migration, while 12,13-EpOME was without effect (Fig. 7**g**). These observations indicate that while the increased accumulation of neutrophils in sEH-deficient skin could be attributed to the increase in LTB4 levels, both 12,13-EpOME and LTB4 contribute to neutrophil activation.

3. Discussion

A recent first-in-human study using the sEH inhibitor GSK2256294, reported that an adverse effect of the compound was contact dermatitis [26]. The present investigation took a more detailed look at sEH in the skin and identified an important role for the enzyme in keratinocyte proliferation and differentiation. Moreover, sEH deletion aggravated imiquimod-induced psoriasis and sensitized mice to damage induced by mechanical skin stripping. The deletion and inhibition of the sEH had particularly marked effects on levels of 12,13-EpOME/DiHOME and LTB4 to promote vascular permeability and neutrophil infiltration as well as neutrophil activation.

The lipid composition of the epidermis makes a decisive contribution to its barrier function [43], consistent with active PUFA metabolism, keratinocytes express a number of CYP enzymes [44,45]. As substrates the latter use endogenous PUFAs such as linoleic acid, which is used to treat a variety of dermatological disorders (for review see [45]). It is therefore not surprising that the altered expression of several CYP enzymes e.g., CYP2S1 [46], CYP2E1 [47], CYP1A1 and CYP1B1 [48], has been reported in psoriasis and following exposure to UV light which could suggest a potential link between CYP activity and skin inflammation. While we did not assess changes in CYP expression in the current study we did detect an increase in 12-HHT in mechanically damaged stripped skin. The latter mediator can be produced as a

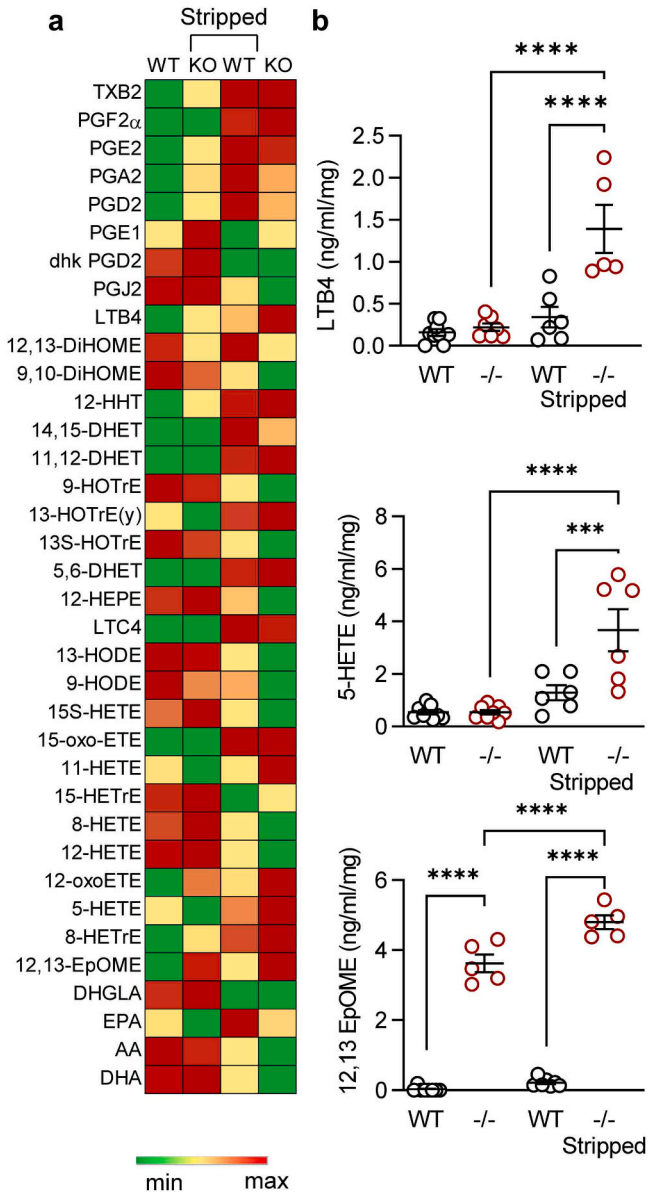

Fig. 6. Effect of stripping on the eicosanoid profile of dorsal skin from wild-type and sEH$^{-/-}$ mice. (**a**) Heat map showing the eicosanoid profile in untreated dorsal skin from wild-type (WT) and sEH$^{-/-}$ (KO) mice and 16 h after depilation and mechanical stripping; n = 6 mice per group. (**b**) Levels of LTB4, 5-HETE, and 12,13-EpOME from the same dataset. * **P < 0.001, * ** *P < 0.0001. AA, arachidonic acid; DHA, docosahexaenoic acid; HDP, dihydroxyocosapentaenoic acid; DHET, dihydroxyicosatrienoic acid; DHGLA, dihomo-γ-linoleic aid; DiHOME, dihydroxyoctadecenoic acid; EET, epoxyeicosatrienoic acid; EPA, eicosapentaenoic acid; EpOME, epoxyoctadecenoic acid; HDHA hydroxydocosahexaenoic acid; HEPE, hydroxy-5Z,8Z,10E,14Z,17Z-eicosapentaenoic acid; HETE, hydroxyeicosatetraenoic acid; HODE, hydroxy-10E,12Z-octadecadienoic acid; HOTrE, hydroxy-10E,12Z,15Z-octadecatrienoic acid; HpODE, hydroperoxy-9Z,11E-octadecadienoic acid; LA, linoleic acid; LTB4, leukotriene B4; oxoETE, oxo-eicosatetraenoic acid; PG, prostaglandin; TX, thromboxane.

byproduct of TxA_2 generation by thromboxane synthase as well as by CYP2S1 [49,50]. Given the high expression of CYP2S1 in psoriasis [46], we have indirect evidence for the activation of this enzyme that supports previous observations. The focus of our study was, however, on an enzyme downstream of CYPs i.e., the sEH.

We focused on the sEH largely because one side-effect of sEH inhibitor treatment was contact dermatitis [26]. However, there are at least two epoxide hydrolases expressed in human and murine skin i.e. sEH (gene name *Ephx2*) and epoxide hydrolase 3 (*Ephx3*) [23–25]. There is probably a role for both enzymes in skin homeostasis as Ephx3 is thought to contribute to the generation of trihydroxy-linoleic acid ceramides [51] that may well affect skin barrier function as trans-epidermal water loss was modestly elevated in Ephx3$^{-/-}$ pups [52]. However, the mediators generated by the two enzymes are distinct and adult Ephx3$^{-/-}$ mice demonstrated no changes in the skin epoxide:diol ratio profile versus wild-type mice [53], and no deficiency in EpOME-derived plasma diols [52].

Among the few studies that have assessed the consequences of sEH inhibition in the skin, most have focused on the microvasculature. Indeed, consistent with the identification of the arachidonic acid epoxide; 11,12-EET, as a vasodilator [3,4], the topical application of a sEH inhibitor was found to increase thermal hyperemia in the skin of diabetic mice, an index of endothelium-dependent microvascular reactivity [54]. Also, sEH inhibition accelerated wound closure [55,56], and increased the vascularization of engineered skin grafts after transplantation [57], findings that fit well with the known link between PUFA epoxides and angiogenesis [58]. The results from this study now indicate that the sEH expressed in keratinocytes can regulate the numbers of CK14 + cells, which are characteristic of the basal keratinocyte layer, as well as CK10 + cells, which are in the spinous layer. As the thickness of the stratum corneum and the number of involucrin-expressing keratinocytes therein were also increased, it appears that PUFA epoxides and diols can affect all stages of epidermal stratification and terminal differentiation. A range of PUFA mediators were affected by sEH deletion/inhibition including 5,6-, 11,12- and 14,15-EET which were previously reported to increase the activity (in vitro) of transglutaminase which is needed to cross-link keratinocyte proteins to make the cornified cell envelop [28]. Other altered mediators included 13 (S)-HODE, which is important for keratinocyte proliferation and differentiation [29,59,60], and PGE_2, which is a growth-promoting autacoid for the epidermis [30]. The epoxide /diol pair most affected by altering sEH activity i.e. 12,13-EpOME/DiHOME has no known links to keratinocytes. However, we did previously report that the activity of the sEH in hair follicle changes during the hair follicle cycle and impacts on two stem cell populations, i.e., hair follicle stem cells and matrix cells to affect telogen to anagen transition and hair growth [61]. Moreover, 12, 13-EpOME (but not 12,13-DiHOME) significantly increased hair shaft growth in isolated anagen-stage hair follicles.

There is significant crosstalk among branches of the arachidonic cascade and selective modulation of COX, LOX, or sEH activity affects flux through the other pathways. Indeed, sEH inhibition and deletion have frequently been reported to result in an increase in COX [62] and LOX products [63,64]. Moreover, the dual inhibition of sEH and 5-LOX inhibited the LPS-induced adhesion of leukocytes to endothelial cells in vitro [65], and was found to be beneficial in carrageenan-induced rat paw edema [66], as well as demonstrating clear anti-inflammatory and anti-fibrotic effects in a murine model of kidney injury [67]. Also, targeting both FLAP and the sEH inhibited cysteinyl-LT and LTB_4 formation and suppressed neutrophil infiltration in a zymosan-induced peritonitis model in mice [68]. What underlies this intimate relationship between LOX and the sEH is not entirely clear but it seems that the sEH is able to metabolize products of the LOX enzymes. For example, in the liver, the sEH hydrolyses hepoxilin A_3 and B generated by 12-LOX [69]. Also, while LTA4H generates LTB4 from LTA4, the sEH has been reported to produce 5 S, 6R-dihydroxy-7,9-*trans*-11,14-cis-eicosatetraenoic acid (5 S,6R-DHETE) from LTA4 [70]. Thus, a possible reason for the increase in LTB4 production following sEH deletion or inhibition could be increased metabolism of LTA4 by LTA4H, even though neither mechanical stripping nor sEH deletion had an impact on *Lta4h* expression.

Given our observations and the increase in skin thickness associated with the loss of sEH activity, it was logical to assess sEH levels in psoriasis. While the expression of CYP enzymes is known to increase in human skin lesions [71], the expression of the sEH decreased. The

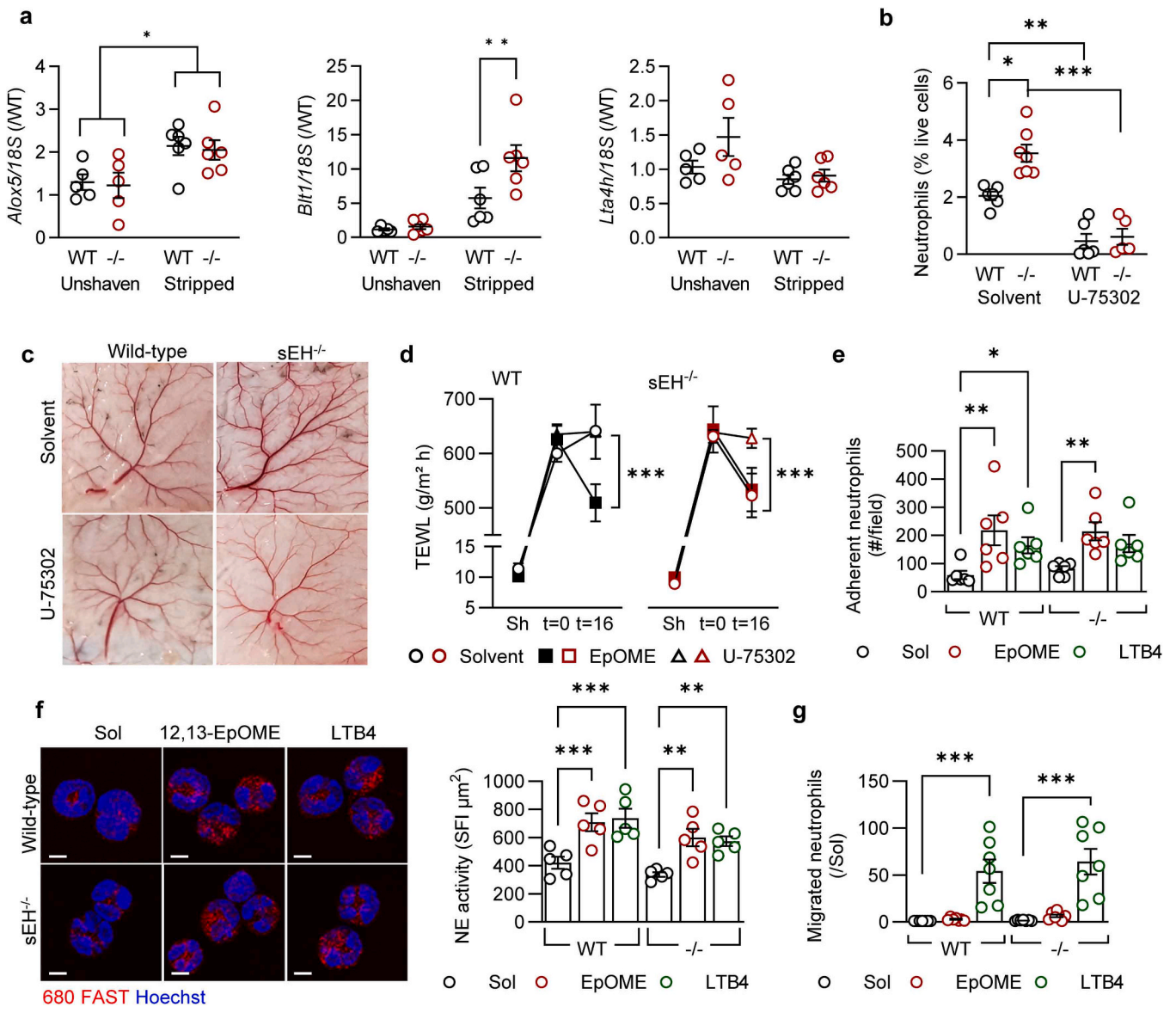

Fig. 7. Effects of 12,13-EpOME and the LTB4 receptor antagonist on neutrophil infiltration and trans epidermal water loss. (**a**) Expression of *Alox5*, *Blt1* and *Lta4h*, relative to 18 S, in unshaven and stripped skin from wild-type (WT) and sEH$^{-/-}$ (-/-) mice; n = 5–6 animals per group (two way ANOVA and Uncorrected Fisher's LSD test). (**b**) Neutrophil (CD45 +CD11b+Ly6G+ cells) infiltration into dorsal skin 16 h after stripping-induced inflammation in animals treated with solvent (Sol) or the BLT1 antagonist U-75302; n = 5–7 mice per group (two way ANOVA and uncorrected Fisher's LSD test). (**c**) Representative images from the underside of skin from wild-type (WT) and sEH$^{-/-}$ (-/-) mice treated either with solvent or U-75302 after stripping. Comparable results were obtained using 4 additional animals in each group. (**d**) Transepidermal water loss (TEWL) in dorsal skin of wild type (WT), and sEH$^{-/-}$ mice measured after shaving (Sh), immediately after shaving and stripping (t = 0) and again after 16 h. Mice were treated with either solvent, 12,13-EpOME or U-75302 immediately after stripping; n = 4–6 mice per group, group (two way ANOVA and uncorrected Fisher's LSD test). (**e**) Adhesion of bone marrow-derived neutrophils from wild-type (WT) and sEH$^{-/-}$ (-/-) mice to recombinant ICAM-1 in the presence of solvent (Sol), 12,13-EpOME or LTB4; n = 5–6 mice per group (two way ANOVA and uncorrected Fisher's LSD test). (**f**) Neutrophil elastase activity (680-FAST surface fluorescent intensity) in bone marrow-derived neutrophils treated with solvent (Sol), 12,13-EpOME or LTB4 for 30 min. Bar = 5 µm; n = 5 mice per group with 30–50 cells/mouse (two way ANOVA and uncorrected Fisher's LSD test). (**g**) Neutrophil migration through mouse lung endothelial cells in the presence of solvent (Sol), 12,13-EpOME or LTB4; n = 6–7 mice per group (two way ANOVA and uncorrected Fisher's LSD test). *P < 0.05, * *P < 0.01, * **P < 0.001.

application of imiquimod to wild-type mice to induce psoriasis increased skin thickness and stimulated CK14 + keratinocyte proliferation. As these hallmarks of psoriasis, including the appearance of neutrophil rich micro-abscesses were even more pronounced in sEH$^{-/-}$ mice, it is tempting to speculate that a decrease in sEH contributes to disease pathology. Imiquimod-induced psoriasis is reported to be driven by T cells, particularly αβ T-cells and δγ T-cells [34], but T cell infiltration was attenuated rather than enhanced in psoriatic skin from sEH-deficient mice. The infiltration of neutrophils and macrophages was, on the other hand, more pronounced than in wild-type mice. Thus, the immune cell response in sEH$^{-/-}$ mice was distinct from that usually observed in this model. As a consequence, we studied a model of atopic dermatitis linked with mechanical stress-induced inflammation that is reportedly reliant on neutrophil infiltration [37]. Also in this model, the injury was more pronounced in sEH$^{-/-}$ mice and mild mechanical stress induced by shaving or more severe stress induced by stripping led to pronounced vascular leak and neutrophil infiltration.

Several PUFA-derived mediators were generated in response to mechanical stress but only 5-HETE, 12,13-EpOME/DiHOME and LTB4 were altered in an sEH-dependent manner. This was not entirely expected as

LTB4 levels were previously reported to be unaltered in a similar model of skin damage induced by tape stripping [72]. LTB4 has well-characterized effects on neutrophil recruitment and activation [40,73], including the generation of the pro-inflammatory cytokines TNF-α and IL-6 [74], and antagonizing its receptor i.e. BLT1, effectively prevented neutrophil recruitment induced by mechanical stripping. It was not possible to assess cytokine expression in the current study but sEH inhibition increases levels of the PUFA epoxide, 11,12-EET, which is known to prevent nuclear factor κ-B activation and prevent TNF-α generation to exert its anti-inflammatory effect [5]. However, our data did reveal that there is likely to be a role for both LTB4 and 12, 13-EpOME in the skin inflammatory response. Even though the linoleic acid epoxide did not stimulate neutrophil migration, it was able to increase neutrophil elastase activity as well as adherence to endothelial cells. Our observations are, therefore, consistent with previous reports indicating that 12,13-EpOME can increase the neutrophil respiratory burst during an allergic reaction [75]. The lack of sEH not only means that 12,13-EpOME levels increased but also that the levels of 12, 13-DiHOME decreased. This is relevant inasmuch as DiHOMEs have been reported to suppress the neutrophil respiratory burst by an as yet unclarified mechanism [75,76]. Taken together, our results show that the sEH plays an important role in skin homeostasis and that a decrease in its expression/activity sensitizes the skin, making it more prone to chemical or mechanical stress-induced dermatitis. These observations should be taken into account in future clinical studies using sEH inhibitors.

4. Methods

4.1. Animals

C57BL/6(N) mice were purchased from Charles River (Sulzfeld, Germany) and sEH reporter mice (Ephx2-e(Loxp-cc-TGA-STOP-Loxp-cc-2A-tdTomato-WPRE-pA)1 were generated by Shanghai Model Organisms (Shanghai, China). Floxed sEH mice (Ephx2tm1.1Arte) were generated by TaconicArtemis GmbH (Cologne, Germany) as described [77], and crossed with animals expressing Cre under the control of the endogenous Gt(ROSA)26Sor promoter (TaconicArtemis GmbH) to generate mice lacking the sEH in all tissues ($sEH^{-/-}$). In some experiments, wild-type mice were treated with the sEH inhibitor N-[1-(1-Oxopropyl)− 4-piperidinyl]-N′-[4-(trifluoromethoxy)phenyl] urea (TPPU) for 4 days (dissolved in DMSO and then added to 250 μL PLO Base to give a final concentration of 30 μmol/L) [78]. All animals were housed in conditions that conform to the guide for the care and use of laboratory animals in accordance with EU Directive 2010/63/EU as amended by Regulation (EU) 2019/1010 for animal experiments. Both the University Animal Care Committee and the Federal Authority for Animal Research at the Regierungspräsidium Darmstadt (Hessen, Germany) approved the study protocol (FU 2001). For the isolation of organs, mice were sacrificed using 4% isoflurane in air followed by cervical dislocation.

4.2. Induction of psoriasis

Psoriasis was induced in 8–10 week-old male mice using imiquimod as described [34]. Briefly, an area (approximately 2 ×2.5 cm) of dorsal skin was shaved one day before the topical application of 5% imiquimod (Aldara cream; 3 M Pharmaceuticals, Solna, Sweden). The cream was re-applied daily for 3 or 6 days. Skin thickness was measured using a vernier caliper every day and skin was harvested immediately after shaving (day 0) as well as on days 3, 6 and 10.

4.3. Mechanically-induced inflammation (tape stripping)

Dermatitis was induced in an area (approximately 2.5 ×2 cm) of dorsal skin by the combination of depilatory cream (Reckitt Benckiser Deutschland GmbH, Heidelberg, Germany) followed by mechanical stripping (15 times) with adhesive tape (3 M Tegaderm, Westnet Inc, Canton, MA) as outlined [79]. In some experiments mice were treated topically with ~250 μL transderma Plo gel ultramax base (Cat#TR220, Transderma Pharmaceuticals, Coquitlam, Canada) containing solvent (0.3% DMSO), 12,13-EpOME (30 μmol/L/mouse) or U-75302 (10 μg/mouse; Cat# 70705, Cayman, Ann Arbor, MI) immediately after and 6 h after stripping. Samples were then collected after 16 h.

4.4. Evaluation of blood vessel leakage

Animals were injected intravenously with Evans blue dye (200 μL of 0.5% Evans blue dye in PBS; Sigma-Aldrich, Darmstadt Germany) as described [80]. After 15 min animals were sacrificed and skin samples were collected, photographed and weighed. Then Evans blue was extracted overnight (56 °C) under constant agitation using formamide (#47671, Sigma-Aldrich, Darmstadt, Germany). The amount of dye extracted was measured with a spectrophotometer (absorbance at λ610 nm) and normalized to the wet weight of the tissue.

4.5. Measurement of trans-epidermal water loss

Measurement of trans-epidermal water loss was measured on the dorsal skin lesion of mice immediately after shaving and stripping, and again after 16 h using a Tewameter TM300 (Courage & Khazaka Electronic GmbH, Cologne, Germany). Three sites on the dorsal skin were assessed and averaged for each animal.

4.6. Immunohistochemistry

4.6.1. Murine skin

Samples were fixed with 4% paraformaldehyde (PFA) overnight at 4 °C. After fixation samples were dehydrated by sequential washing in 70%, 80%, and 95% alcohol (45 min each), followed by 3 washes in 100% alcohol (1 h each). Samples were cleared by washing with xylene (2 ×1 h). Finally, samples were washed in paraffin (3 ×1 h) and embedded in paraffin blocks. Skin Section (5 μm) were cut and dried overnight at 37 °C. Sample slides were deparaffinized by washing (2 ×10 min) with xylene. Slides were then sequentially placed in graded ethanol baths i.e. 100% to 95%, 70% and 50% ethanol and water (5 min each) for rehydration before being placed in a steamer in the presence of citrate buffer for 20 min to demask the antigens. Then samples were placed on ice (10 min) before being blocked with donkey serum (5% in 0.3% Triton X-100, 1 h) and incubated overnight with primary antibodies (4 °C). Primary antibodies used were as follows: cytokeratin 14 (1:200, Cat# 906004, clone: Poly9060, Biolegend, San Diego, UK), cytokeratin 10 (1:200, Cat# ab76318, Clone: EP1607IHCY, abcam, Berlin, Germany), involucrin (1:150, Cat# 924401, clone: PRB140C, Biolegend, San Diego, UK) and Ki67 (1:100, Cat# ab16667, clone: SP6, abcam, Berlin, Germany). To visualize the vasculature, fixed samples were embedded in Tissue-Tek (Cat# 4583, Sakura Torrance, CA) and 100 μm cryo-sections were made and stained for anti-CD31 (1:100, Cat# DIA 310, clone: SZ31, Dianova, Hamburg, Germany) and anti-Lyve1 (1:100, Cat# AF2125, R&D, Abingdon, UK). Thereafter, primary antibody samples were removed and samples were incubated with respective alexaFlour-conjugated secondary antibodies for 60–90 min at room temperature. Sections were washed, and nuclei were counterstained with Hoechst 33342 (Sigma-Aldrich, Darmstadt, Germany). Imaging was performed with Zeiss confocal laser scanning microscope-780 (Jena, Germany). All images were analyzed by Imaris (verion 9.6.0 Bitplane AG, Zurich, Switzerland).

4.6.2. Human skin

Paraffin embedded skin sections from healthy individuals and from subjects with psoriasis were obtained from BioCat GmbH (Cat# HP-101-ZY and cat# SKI06-PT, Heidelberg, Germany). Samples were rehydrated

as described above and incubated with a polyclonal sEH antibody (1:100, Cat# HPA023094, Sigma Aldrich, Darmstadt, Germany), and detected with a rabbit specific HRP/DAB detection IHC kit (Cat# ab64261, Abcam, Berlin, Germany) according to the manufacturer's instructions.

4.7. Hematoxylin & eosin staining

Dewaxed and rehydrated paraffin Section (5 μm) were stained with hematoxylin (Cat#GHS316 Gill No. 3, Sigma-Aldrich, Darmstadt, Germany) for 3 min, before being washed in running water for 10 min followed by staining with eosin (Cat#R03040, Sigma-Aldrich, Darmstadt, Germany) for 30 s. Finally, samples were dehydrated and mounted with entallon (Cat# 1.07960, Sigma-Aldrich, Darmstadt, Germany).

4.8. Immunoblotting

Skin samples were lysed in Triton X-100 buffer enriched with protease and phosphatase inhibitors. Samples were separated by SDS-PAGE and subjected to Western blotting and detection was performed by enhanced chemiluminescence using a commercially available kit (Amersham, Freiburg, Germany) as described [81].

4.9. Skin digestion and FACS analyses

To generate a single cell suspension from skin, subcutaneous fat was removed and skin was chopped into 1 mm pieces which were then incubated in liberase (300 μg/mL; Cat# 5401119001, Sigma-Aldrich, Darmstadt, Germany) and DNase 1 digestion cocktail (50 U/mL, Cat# Roche-11284932001, Sigma-Aldrich, Darmstadt, Germany) for 60–90 min at 37 °C as described [82]. Digested skin cells were passed through a 100 μm pore filter and then through a 40 μm pore filter. The single cells obtained were washed once in 1%BSA and then blocked with FcR blocking reagent (Cat# 101302, Biolegend, San Diego, US) for 10 min. Thereafter, cells were incubated with fluorochrome-conjugated antibodies and analyzed using a LSR II/Fortessa flow cytometer (BD, Heidelberg, Germany). Data were analyzed using FlowJo Vx (TreeStar, Williamson Way, UK). All antibodies and secondary reagents were titrated to determine optimal concentrations. Comp-Beads (#A10513, Thermo Fisher Scientific, Dreieich, Germany were used for single-color compensation to create multicolour compensation matrices. The instrument calibration was controlled daily using Cytometer Setup and Tracking beads (BD Biosciences, Heidelberg, Germany).

The following antibodies were used to characterize immune cell subsets in skin: anti-CD3-PE-CF594 (Cat# 562286), anti-CD4-BV711 (Cat# 563050), anti-CD8-BV650 (Cat# 100742), anti-CD11b-BV605 (Cat# 101257), anti-CD11c-AlexaFluor700 (Cat# 560583), anti-CD19-APC-H7 (Cat# 560143), anti-CD326-BV711 (Cat# 563134), anti-Ly6C-Per-CP-Cy5.5 (Cat# 560525), anti-NK1.1 BV510 (Cat# 563096) all from BD Biosciences (Heidelberg, Germany), anti-CD45-Vio-Blu (Cat# 130–092-910), anti-MHC-II-APC (Cat# 130–102-139), and anti-CD-90.2-PE (Cat# 130–102-489) from Miltenyi Biotec (Bergisch Gladbach Germany) and anti-F4/80-PE-Cy7 (Cat# 123114), anti-GITR-FITC (Cat# 126308), anti-gd TCR APC (Cat# 118116), and anti-Ly6G-APC Cy7 (Cat# 127624) from BioLegend (San Diego, CA, USA).

4.10. RNA isolation, cDNA synthesis and RT-qPCR

Total RNA was extracted from healthy and inflamed skin tissues using peqGold TriFast reagent (Cat#30–2010, VWR, Darmstadt, Germany) according to the manufacture's protocol. RNA (1 μg) was used for reverse transcription reaction to make cDNA by using SuperScript IV kit (Cat#18091050, Thermofischer scientific, Dreieich, Germany) according to the manufacturer's protocol. Gene specific primers (BioSpring GmbH, Germany) were designed using primer BLAST [83]. The primers used were as follows: 5-LOX: forward GTATCGCCATGTACCGCCAG, reverse GTTCCCGGGCCTTAGTGTTG, BLT1: forward CAGGACCCTGGCACTAAGAC, reverse CAGGAGAAGAAGGTGCTGCA, and 18 S: forward CTTTGGTCGCTCGCTCCTC, reverse CTGACCGGGTTGGTTTTGAT. cDNA was amplified using the Biozym Blue S′Green qPCR kit (Cat#331416XL Biozym, Hessisch Oldendorf, Germany) and a real-time thermal cycler (Agilent Technologies Mx3000, USA). All RNAs were normalized to 18 S rRNA.

4.11. Keratinocyte culture and differentiation

Human epidermal primary keratinocytes were obtained from Lifeline Cell Technology (Cat# FC-0025; Frederick, Maryland) and cultured in Dermalife calcium-free basal medium (Cat # L0008,) supplemented with rh-insulin factor (5 μg/mL; Cat# LS-1004), L-glutamine (6 mmol/L; Cat# LS1031), epinephrine (1 μmol/L; Cat# LS-1032), apo-transferrin (5 μg/mL; Cat# LS-1033), rhTGF-α (0.5 ng/mL; Cat# LS-1034), extract P (0.4%; Cat# LS-1037) and hydrocortisone hemisuccinate (100 ng/mg; Cat# LS-1039; all from Lifeline Cell Technology). Keratinocytes were differentiated with calcium (2 mmol/L) for 48 h before harvesting and processing to measure sEH activity.

4.12. sEH activity assay

Soluble epoxide hydrolase activity was determined in dorsal skin samples and cells lysates (5 μg) treated with solvent or the sEH inhibitor *trans*-4-[4-(3-adamantan-1-ylureido)cyclohexyloxy]-benzoic acid (*t*-AUCB) [84] as previously described [85]. Reactions were performed in 100 μL of potassium phosphate buffer (100 mmol/L, pH 7.2) and started by the addition of 12,13-EpOME (0.25 μmol/L). After 10 min (37 °C) reactions were stopped by placing the samples on ice followed by immediate extraction (twice) with ethyl acetate (0.5 mL). For liquid chromatography–tandem mass spectrometry (LC–MS/MS), one-tenth of the sample was spiked with a deuterated internal standard i.e., d4 12, 13-diHOME/DiHOME (Cayman, Hamburg, Germany). After evaporation of the solvent in a vacuum block under a gentle stream of nitrogen, the residues were reconstituted in 50 μL of acetonitrile:water (1:1, v/v) and analyzed with a Sciex API4000 mass spectrometer operating in multiple reaction monitoring (MRM) mode. Chromatographic separation was performed on a Gemini C18 column (150 × 2 mm I.D., 5 μm particle size; Phenomenex, Aschaffenburg, Germany).

4.13. PUFA metabolite profiling (LC-MS/MS)

Skin samples (30–40 mg) were ground under liquid N2 and were extracted with 1 mL ethyl acetate, vortexed for 20 s, placed on ice for 10 min, vortexed again and subsequently centrifuged (10,000 g, 5 min, 4 °C) as described [86]. The upper phase was collected and the ethyl acetate extraction was performed again. Samples were spiked with a deuterated internal standard mix (8,9-DHET-d11, 11,12-DHET-d11, 14, 15-DHET-d11, 9,10-DiHOME-d4, 12,13-DiHOME-d4, 5,6-EET-d11, 8, 9-EET-d8, 11,12-EET-d8, 14,15-EET-d8, 9.10-EpOME-d4, 12, 13-EpOME-d4, 5S-HETE-d8, 12S-HETE-d8, 15S-HETE-d8, 20-HETE-d6, 9S-HODE-d4, 13S-HODE-d4, all from Cayman, Hamburg, Germany). Both upper phase samples were combined and evaporated to dryness in a vacuum manifold under a continual nitrogen stream. The residues were reconstituted with 50 μL of acetonitrile:water (50:50, v/v, containing 100 ng/mL flufenamic acid as internal control) and analyzed using a Sciex QTrap5500 mass spectrometer operating in multiple reaction monitoring (MRM) mode in negative ionization mode. ESI parameters were set to CUR: 24 psi, IS: − 4500 V, TEM: 600 °C, GS1: 45 psi, GS2: 60 psi. Chromatographic separation was performed on an Agilent 1290 Infinity LC system (Agilent, Waldbronn, Germany), using a Gemini C18 column (150 ×2 mm I.D., 5 μm particle size; Phenomenex, Aschaffenburg, Germany). The mobile phase consisted of (A) water + 0.0125% ammonia and (B) acetonitrile + 0.0125% ammonia. Elution of analytes was carried out under gradient conditions at a flow rate of

0.5 mL/min going from 15% B to 40% B in 10 min, increasing to 90% B in 2 min, hold 90% B for 1 min, and equilibrated in 15% B for 5.5 min 10 μL of each sample was injected onto the column. The column temperature was kept at 40 °C. Samples were kept in the autosampler at 6 °C until analysis. For the preparation of calibration curves, stock solutions were prepared in ethanol that contained primary fatty acids and oxylipin standards. Working standard solutions were prepared by serial dilution of the stock solutions to create the necessary concentrations. All samples and dilutions of the standards were spiked with internal deuterated standards: Metabolite concentrations were determined by reference to the standards. Analyst 1.6.2 and MultiQuant 3.0 (both Sciex, Darmstadt, Germany), were used for data acquisition and analysis, respectively.

4.13.1. Isolation and culture of murine neutrophils

Murine neutrophils were isolated from the marrow of both the front and hindlimbs as described [87]. Briefly, bone marrow was flushed out using PBS containing 0.5% BSA and 2 mmol/L EDTA. Cells were carefully loaded onto a discontinuous Percol gradient (52%64%72%, Cat#17–0891-01, VWR, Dublin, Ireland) and centrifuged (1000 g without break and acceleration, 4 °C) for 30 min. Neutrophils were collected from the 64%/72% interface and washed once with PBS. Any remnant red blood cells were lysed using an erythrocyte lysis buffer. Isolated neutrophils were kept in RPMI 1640 medium (Cat#21875–091, Gibco, Dreieich, Germany) supplemented with 10% FCS at 37 °C in the presence of 5% CO_2.

4.13.2. In vitro neutrophil adhesion assay

Eight-well glass chamber slides were coated with human recombinant ICAM-1 (Cat#150–05, PeproTech, Heidelberg, Germany overnight at 4 °C. Glass chambers were later blocked with 10% BSA for 1 h at room temperature. Then 5×10^4 cells were added to the blocked chambers, treated with either DMSO (0.1%), LTB4 (100 nmol/L) or 12,13-EpOME (10 μmol/L) and allowed to adhere for 30 min, before being fixed with 4% PFA and labeled with a Ly6G antibody (#551459, 1A8, BD bioscience, Heidelberg, Germany). Adherent Ly6G+ cells were imaged using a Leica Stellaris laser scanning microscope (Leica Microsystems, Wetzlar, Germany) and analyzed using Imaris software (version 9.6.0 Bitplane AG, Zurich, Switzerland).

4.13.3. In vitro neutrophil elastase enzymatic activity assay

Isolated neutrophils were seeded on ICAM-1 coated slides (Cat#150–05, Peprotech, East Windsor, United States), and treated with solvent (DMSO 0.1%), LTB4 (100 nmol/L) or 12,13-EpOME (10 μmol/L) or in the presence of neutrophil elastase 680-FAST (2 μmol/L per well; Cat# NEV11169, PerkinElmer, Hamburg, Germany) for 30 min. Afterward slides were washed, fixed, labeled with a Ly6G antibody and analyzed by confocal microscopy as described above.

4.13.4. Transendothelial cell migration

Murine lung endothelial cells were isolated and cultured as described [81], before being seeded on a fibronectin coated trans-well filters (3 μm pore size; BD Pharmingen, Franklin lakes, USA). Once confluent, endothelial cells were stimulated with tumor necrosis factor α (10 ng/mL; Cat# 315–01 A, Peprotech, Hamburg, Germany) for 5 h. After careful washing, neutrophils (1×10^5 cells) were added on top of the endothelial cell monolayer and allowed to migrate towards the lower chamber containing either solvent (0.1% DMSO), 12,13-EpOME (10 μmol/L or LTB4 (100 nmol/L) for 3 h. Migrated neutrophils were collected and counted by flow cytometry (BD FACSVerse, BD, Heidelberg, Germany).

4.14. Statistical analysis

Data are expressed as mean ± SEM. Statistical evaluation was performed with GraphPad Prism (version 9.1.0) using Student's t test for unpaired data, one-way ANOVA followed by Tukey's multiple comparison test, or two-way ANOVA followed by Sidak's multiple comparison test or an Uncorrected Fisher's LSD test where appropriate. Values of $P < 0.05$ were considered statistically significant.

Funding

This work was supported by the Deutsche Forschungsgemeinschaft (SFB1039/3 B6 - project ID 204083920, and GRK 2336 TP5 - Project ID 321115009. B.D.H was supported by NIH – NIEHS (RIVER Award) R35 ES030443–01 and NIH – NIEHS (Superfund Award) P42 ES004699.

CRediT authorship contribution statement

Huard Arnaud: Investigation. **Hu Jiong:** Investigation. **Naeem Zumer:** Conceptualization, Data curation, Formal analysis, Investigation, Writing – original draft. **Zukunft Sven:** Formal analysis. **Frömel Timo:** Conceptualization, Data curation, Formal analysis, Supervision. **Fleming Ingrid:** Conceptualization, Funding acquisition, Project administration, Supervision, Writing – original draft, Writing – review & editing. **Hammock Bruce D:** Resources. **Weigert Andreas:** Methodology, Writing – review & editing.

Declaration of Competing Interest

The authors declare the following financial interests/personal relationships which may be considered as potential competing interests: Ingrid Fleming reports financial support was provided by Deutsche Forschungsgemeinschaft (SFB1039 B6 - project ID 204083920). Ingrid Fleming reports a relationship with Deutsche Forschungsgemeinschaft (GRK 2336 TP5 - Project ID 321115009) that includes: funding grants.

Data availability

Data will be made available on request.

Acknowledgements

The authors are indebted to Orwa Barakat and Oliver Haun for expert technical assistance.

Appendix A. Supporting information

Supplementary data associated with this article can be found in the online version at doi:10.1016/j.biopha.2024.116127.

References

[1] I. Fleming, The pharmacology of the cytochrome P450 epoxygenase/soluble epoxide hydrolase axis in the vasculature and cardiovascular disease, Pharm. Rev. 66 (2014) 1106–1140, https://doi.org/10.1124/pr.113.007781.
[2] K.-D. Ni, J.-Y. Liu, The functions of cytochrome P450 ω-hydroxylases and the associated eicosanoids in inflammation-related diseases, Front Pharm. 12 (2021) 716801, https://doi.org/10.3389/fphar.2021.716801.
[3] B. Fisslthaler, R. Popp, L. Kiss, M. Potente, D.R. Harder, I. Fleming, R. Busse, Cytochrome P450 2C is an EDHF synthase in coronary arteries, Nature 401 (1999) 493–497, https://doi.org/10.1038/46816.
[4] W.B. Campbell, D. Gebremedhin, P.F. Pratt, D.R. Harder, Identification of epoxyeicosatrienoic acids as endothelium-derived hyperpolarizing factors, Circ. Res 78 (1996) 415–423, https://doi.org/10.1161/01.res.78.3.415.
[5] K. Node, Y. Huo, X. Ruan, B. Yang, M. Spiecker, K. Ley, D.C. Zeldin, J.K. Liao, Anti-inflammatory properties of cytochrome P450 epoxygenase-derived eicosanoids, Science 285 (1999) 1276–1279, https://doi.org/10.1126/science.285.5431.1276.
[6] I. Fleming, New lipid mediators in retinal angiogenesis and retinopathy, Front Pharm. 10 (2019) 739, https://doi.org/10.3389/fphar.2019.00739.
[7] T. Frömel, Z. Naeem, L. Pirzeh, I. Fleming, Cytochrome P450-derived fatty acid epoxides and diols in angiogenesis and stem cell biology, Pharm. Ther. (2021) 108049, https://doi.org/10.1016/j.pharmthera.2021.108049.
[8] N. Chiamvimonvat, C.-M. Ho, H.-J. Tsai, B.D. Hammock, The soluble epoxide hydrolase as a pharmaceutical target for hypertension, J. Cardiovasc Pharm. 50 (2007) 225–237, https://doi.org/10.1097/FJC.0B013E3181506445.
[9] A. Cronin, S. Mowbray, H. Dürk, S. Homburg, I. Fleming, B. Fisslthaler, F. Oesch, M. Arand, The N-terminal domain of mammalian soluble epoxide hydrolase is a

phosphatase, Proc. Natl. Acad. Sci. USA 100 (2003) 1552–1557, https://doi.org/10.1073/pnas.0437829100.
[10] J.W. Newman, C. Morisseau, T.R. Harris, B.D. Hammock, The soluble epoxide hydrolase encoded by EPXH2 is a bifunctional enzyme with novel lipid phosphate phosphatase activity, Proc. Natl. Acad. Sci. USA 100 (2003) 1558–1563, https://doi.org/10.1073/pnas.0437724100.
[11] J. Kramer, E. Proschak, Phosphatase activity of soluble epoxide hydrolase, Prostaglandins Other Lipid Mediat 133 (2017) 88–92, https://doi.org/10.1016/j.prostaglandins.2017.07.002.
[12] T. Frömel, J. Hu, I. Fleming, Lipid mediators generated by the cytochrome P450-Epoxide hydrolase pathway, Adv. Pharm. 97 (2023) 327–373, https://doi.org/10.1016/bs.apha.2022.12.004.
[13] A. Das Mahapatra, R. Choubey, B. Datta, Small molecule soluble epoxide hydrolase inhibitors in multitarget and combination therapies for inflammation and cancer, Molecules 25 (2020) 5488, https://doi.org/10.3390/molecules25235488.
[14] J. Lai, C. Chen, The role of epoxyeicosatrienoic acids in cardiac remodeling, Front Physiol. 12 (2021) 642470, https://doi.org/10.3389/fphys.2021.642470.
[15] Y. Wang, K.M. Wagner, C. Morisseau, B.D. Hammock, Inhibition of the soluble epoxide hydrolase as an analgesic strategy: a review of preclinical evidence, J. Pain. Res 14 (2021) 61–72, https://doi.org/10.2147/JPR.S241893.
[16] J. Zhang, M. Tu, Z. Liu, G. Zhang, Soluble epoxide hydrolase as a therapeutic target for obesity-induced disorders: roles of gut barrier function involved, Prostaglandins Leukot. Ess. Fat. Acids 162 (2020) 102180, https://doi.org/10.1016/j.plefa.2020.102180.
[17] J.D. Imig, B.D. Hammock, Soluble epoxide hydrolase as a therapeutic target for cardiovascular diseases, Nat. Rev. Drug Discov. 8 (2009) 794–805, https://doi.org/10.1038/nrd2875.
[18] O. Jung, R.P. Brandes, I.-H. Kim, F. Schweda, R. Schmidt, B.D. Hammock, R. Busse, I. Fleming, Soluble epoxide hydrolase is a main effector of angiotensin II-induced hypertension, Hypertension 45 (2005) 759–765, https://doi.org/10.1161/01.hyp.0000153792.29478.1d.
[19] D. Ai, Y. Fu, D. Guo, H. Tanaka, N. Wang, C. Tang, B.D. Hammock, J.Y.-J. Shyy, Y. Zhu, Angiotensin II up-regulates soluble epoxide hydrolase in vascular endothelium in vitro and in vivo, Proc. Natl. Acad. Sci. USA 104 (2007) 9018–9023, https://doi.org/10.1073/pnas.0703229104.
[20] D. Ai, W. Pang, N. Li, M. Xu, P.D. Jones, J. Yang, Y. Zhang, N. Chiamvimonvat, J. Y.-J. Shyy, B.D. Hammock, Y. Zhu, Soluble epoxide hydrolase plays an essential role in angiotensin II-induced cardiac hypertrophy, Proc. Natl. Acad. Sci. USA 106 (2009) 564–569, https://doi.org/10.1073/pnas.0811022106.
[21] J. Hu, S. Dziumbla, J. Lin, S.-I. Bibli, S. Zukunft, J. de Mos, K. Awwad, T. Frömel, A. Jungmann, K. Devraj, Z. Cheng, L. Wang, S. Fauser, C.G. Eberhart, A. Sodhi, B. D. Hammock, S. Liebner, O.J. Müller, C. Glaubitz, H.-P. Hammes, R. Popp, I. Fleming, Inhibition of soluble epoxide hydrolase prevents diabetic retinopathy, Nature 552 (2017) 248–252, https://doi.org/10.1038/nature25013.
[22] J. Hu, S.-I. Bibli, J. Wittig, S. Zukunft, J. Lin, H.-P. Hammes, R. Popp, I. Fleming, Soluble epoxide hydrolase promotes astrocyte survival in retinopathy of prematurity, J. Clin. Invest 129 (2019) 5204–5218, https://doi.org/10.1172/JCI123835.
[23] A.E. Enayetallah, R.A. French, M.S. Thibodeau, D.F. Grant, Distribution of soluble epoxide hydrolase and of cytochrome P450 2C8, 2C9, and 2J2 in human tissues, J. Histochem Cytochem 52 (2004) 447–454, https://doi.org/10.1177/002215540405200403.
[24] M. Decker, M. Adamska, A. Cronin, F. Di Giallonardo, J. Burgener, A. Marowsky, J. R. Falck, C. Morisseau, B.D. Hammock, A. Gruzdev, D.C. Zeldin, M. Arand, EH3 (ABHD9): the first member of a new epoxide hydrolase family with high activity for fatty acid epoxides, J. Lipid Res. 53 (2012) 2038–2045, https://doi.org/10.1194/jlr.M024448.
[25] H. Yamanashi, W.E. Boeglin, C. Morisseau, R.W. Davis, G.A. Sulikowski, B. D. Hammock, A.R. Brash, Catalytic activities of mammalian epoxide hydrolases with cis and trans fatty acid epoxides relevant to skin barrier function, J. Lipid Res. 59 (2018) 684–695, https://doi.org/10.1194/jlr.M082701.
[26] A.L. Lazaar, L. Yang, R.L. Boardley, N.S. Goyal, J. Robertson, S.J. Baldwin, D. E. Newby, I.B. Wilkinson, R. Tal-Singer, R.J. Mayer, J. Cheriyan, Pharmacokinetics, pharmacodynamics and adverse event profile of GSK2256294, a novel soluble epoxide hydrolase inhibitor, Br. J. Clin. Pharm. 81 (2016) 971–979, https://doi.org/10.1111/bcp.12855.
[27] A.C. Kendall, S.M. Pilkington, K.A. Massey, G. Sassano, L.E. Rhodes, A. Nicolaou, Distribution of bioactive lipid mediators in human skin, J. Invest Dematol. 135 (2015) 1510–1520, https://doi.org/10.1038/jid.2015.41.
[28] P.A. Ladd, L. Du, J.H. Capdevila, R. Mernaugh, D.S. Keeney, Epoxyeicosatrienoic acids activate transglutaminases in situ and induce cornification of epidermal keratinocytes, J. Biol. Chem. 278 (2003) 35184–35192, https://doi.org/10.1074/jbc.M301666200.
[29] E. Ogawa, Y. Owada, S. Ikawa, Y. Adachi, T. Egawa, K. Nemoto, K. Suzuki, T. Hishinuma, H. Kawashima, H. Kondo, M. Muto, S. Aiba, R. Okuyama, Epidermal FABP (FABP5) regulates keratinocyte differentiation by 13(S)-HODE-mediated activation of the NF-κB signaling pathway, J. Invest Dermatol. 131 (2011) 604–612, https://doi.org/10.1038/jid.2010.342.
[30] A.P. Pentland, P. Needleman, Modulation of keratinocyte proliferation in vitro by endogenous prostaglandin synthesis, J. Clin. Invest 77 (1986) 246–251, https://doi.org/10.1172/JCI112283.
[31] N. Swain, R.M. Hosalkar, S. Routray, Involucrin, in: S. Choi (Ed.), Encyclopedia of Signaling Molecules, Springer New York, New York, NY, 2017, pp. 1–7.
[32] J.M. Hugh, J.M. Weinberg, Update on the pathophysiology of psoriasis, Cutis 102 (2018) 6–12.
[33] A. Rendon, K. Schäkel, Psoriasis pathogenesis and treatment, Int. J. Mol. Sci. 20 (2019), https://doi.org/10.3390/ijms20061475.
[34] L. van der Fits, S. Mourits, J.S.A. Voerman, M. Kant, L. Boon, J.D. Laman, F. Cornelissen, A.-M. Mus, E. Florencia, E.P. Prens, E. Lubberts, Imiquimod-induced psoriasis-like skin inflammation in mice is mediated via the IL-23/IL-17 axis, J. Immunol. 182 (2009) 5836–5845, https://doi.org/10.4049/jimmunol.0802999.
[35] S. Moos, A.N. Mohebiany, A. Waisman, F.C. Kurschus, Imiquimod-induced psoriasis in mice depends on the IL-17 signaling of keratinocytes, J. Invest Dermatol. 139 (2019) 1110–1117, https://doi.org/10.1016/j.jid.2019.01.006.
[36] P.C. van de Kerkhof, A.M. Lammers, Intraepidermal accumulation of polymorphonuclear leukocytes in chronic stable plaque psoriasis, Dermatologica 174 (1987) 224–227, https://doi.org/10.1159/000249184.
[37] M.K. Oyoshi, R. He, Y. Li, S. Mondal, J. Yoon, R. Afshar, M. Chen, D.M. Lee, H. R. Luo, A.D. Luster, J.S. Cho, L.S. Miller, A. Larson, G.F. Murphy, R.S. Geha, Leukotriene B4-driven neutrophil recruitment to the skin is essential for allergic skin inflammation, Immunity 37 (2012) 747–758, https://doi.org/10.1016/j.immuni.2012.06.018.
[38] A. Onoue, K. Kabashima, M. Kobayashi, T. Mori, Y. Tokura, Induction of eosinophil- and Th2-attracting epidermal chemokines and cutaneous late-phase reaction in tape-stripped skin, Exp. Dermatol. 18 (2009) 1036–1043, https://doi.org/10.1111/j.1600-0625.2009.00899.x.
[39] T. Takahashi, Y. Kimura, K. Niwa, Y. Ohmiya, T. Fujimura, K. Yamasaki, S. Aiba, In vivo imaging demonstrates ATP release from murine keratinocytes and its involvement in cutaneous inflammation after tape stripping, J. Invest Dermatol. 133 (2013) 2407–2415, https://doi.org/10.1038/jid.2013.163.
[40] K. Saeki, T. Yokomizo, Identification, signaling, and functions of LTB4 receptors, Semin Immunol. 33 (2017) 30–36, https://doi.org/10.1016/j.smim.2017.07.010.
[41] R. He, Y. Chen, Q. Cai, The role of the LTB4-BLT1 axis in health and disease, Pharm. Res. 158 (2020) 104857, https://doi.org/10.1016/j.phrs.2020.104857.
[42] P.V. Afonso, M. Janka-Junttila, Y.J. Lee, C.P. McCann, C.M. Oliver, K.A. Aamer, W. Losert, M.T. Cicerone, C.A. Parent, LTB4 is a signal-relay molecule during neutrophil chemotaxis, Dev. Cell 22 (2012) 1079–1091, https://doi.org/10.1016/j.devcel.2012.02.003.
[43] D. Khnykin, J.H. Miner, F. Jahnsen, Role of fatty acid transporters in epidermis: implications for health and disease, Dermatoendocrinol 3 (2011) 53–61, https://doi.org/10.4161/derm.3.2.14816.
[44] K.R. Feingold, The regulation and role of epidermal lipid synthesis, Adv. Lipid Res. 24 (1991) 57–82, https://doi.org/10.1016/b978-0-12-024924-4.50007-9.
[45] N. Ahmad, H. Mukhtar, Cytochrome p450: a target for drug development for skin diseases, J. Invest Dermatol. 123 (2004) 417–425, https://doi.org/10.1111/j.0022-202X.2004.23307.x.
[46] G. Smith, C.R. Wolf, Y.Y. Deeni, R.S. Dawe, A.T. Evans, M.M. Comrie, J. Ferguson, S.H. Ibbotson, Cutaneous expression of cytochrome P450 CYP2S1: individuality in regulation by therapeutic agents for psoriasis and other skin diseases, Lancet 361 (2003) 1336–1343, https://doi.org/10.1016/S0140-6736(03)13081-4.
[47] G. Smith, R.S. Dawe, C. Clark, A.T. Evans, M.M. Comrie, C.R. Wolf, J. Ferguson, S. H. Ibbotson, Quantitative real-time reverse transcription-polymerase chain reaction analysis of drug metabolizing and cytoprotective genes in psoriasis and regulation by ultraviolet radiation, J. Invest Dermatol. 121 (2003) 390–398, https://doi.org/10.1046/j.1523-1747.2003.12354.x.
[48] S.K. Katiyar, M.S. Matsui, H. Mukhtar, Ultraviolet-B exposure of human skin induces cytochromes P450 1A1 and 1B1, J. Invest Dermatol. 114 (2000) 328–333, https://doi.org/10.1046/j.1523-1747.2000.00876.x.
[49] P. Bui, S. Imaizumi, S.R. Beedanagari, S.T. Reddy, O. Hankinson, Human CYP2S1 metabolizes cyclooxygenase- and lipoxygenase-derived eicosanoids, Drug Metab. Dispos. 39 (2011) 180–190, https://doi.org/10.1124/dmd.110.035121.
[50] T. Frömel, K. Kohlstedt, R. Popp, X. Yin, K. Awwad, E. Barbosa-Sicard, A. C. Thomas, R. Lieberz, M. Mayr, I. Fleming, Cytochrome P4502S1: a novel monocyte/macrophage fatty acid epoxygenase in human atherosclerotic plaques, Basic Res. Cardiol. 108 (2013) 319, https://doi.org/10.1007/s00395-012-0319-8.
[51] V.J. Tyrrell, F. Ali, W.E. Boeglin, R. Andrews, J. Burston, J.C. Birchall, J.R. Ingram, R.C. Murphy, V. Piguet, A.R. Brash, V.B. O'Donnell, C.P. Thomas, Lipidomic and transcriptional analysis of the linoleoyl-omega-hydroxyceramide biosynthetic pathway in human psoriatic lesions, J. Lipid Res 62 (2021) 100094, https://doi.org/10.1016/j.jlr.2021.100094.
[52] M.L. Edin, H. Yamanashi, W.E. Boeglin, J.P. Graves, L.M. DeGraff, F.B. Lih, D. C. Zeldin, A.R. Brash, Epoxide hydrolase 3 (Ephx3) gene disruption reduces ceramide linoleate epoxide hydrolysis and impairs skin barrier function, J. Biol. Chem. (2020), https://doi.org/10.1074/jbc.RA120.016570.
[53] S.L. Hoopes, A. Gruzdev, M.L. Edin, J.P. Graves, J.A. Bradbury, G.P. Flake, F.B. Lih, L.M. DeGraff, D.C. Zeldin, Generation and characterization of epoxide hydrolase 3 (EPHX3)-deficient mice, PLoS ONE 12 (2017) e0175348, https://doi.org/10.1371/journal.pone.0175348.
[54] Y. Savina, T. Duflot, F. Bounoure, S. Kotzki, P.-A. Thiebaut, P.-A. Serreau, M. Skiba, J.-M. Picquenot, M. Cornic, C. Morisseau, B. Hammock, L. Imbert, J.-L. Cracowski, V. Richard, M. Roustit, J. Bellien, Impact of the acute local inhibition of soluble epoxide hydrolase on diabetic skin microcirculatory dysfunction, Diab Vasc. Dis. Res 16 (2019) 523–529, https://doi.org/10.1177/1479164119860215.
[55] A.L. Sander, K. Sommer, T. Neumayer, I. Fleming, I. Marzi, J.H. Barker, J. Frank, H. Jakob, Soluble epoxide hydrolase disruption as therapeutic target for wound healing, J. Surg. Res. 182 (2013) 362–367, https://doi.org/10.1016/j.jss.2012.10.034.
[56] A.L. Sander, H. Jakob, K. Sommer, C. Sadler, I. Fleming, I. Marzi, J. Frank, Cytochrome P450-derived epoxyeicosatrienoic acids accelerate wound epithelialization and neovascularization in the hairless mouse ear wound model,

Lange Arch. Surg. 396 (2011) 1245–1253, https://doi.org/10.1007/s00423-011-0838-z.
[57] D.M. Supp, J.M. Hahn, K.L. McFarland, K.A. Combs, K.S.S. Lee, B. Inceoglu, D. Wan, S.T. Boyce, B.D. Hammock, Soluble epoxide hydrolase inhibition and epoxyeicosatrienoic acid treatment improve vascularization of engineered skin substitutes, Plast. Reconstr. Surg. 4 (2016) e1151, https://doi.org/10.1097/GOX.0000000000001151.
[58] I. Fleming, Epoxyeicosatrienoic acids, cell signaling and angiogenesis, Prostaglandins Other Lipid Mediat 82 (2007) 60–67, https://doi.org/10.1016/j.prostaglandins.2006.05.003.
[59] Y. Cho, V.A. Ziboh, 13-Hydroxyoctadecadienoic acid reverses epidermal hyperproliferation via selective inhibition of protein kinase C-beta activity, Biochem Biophys. Res Commun. 201 (1994) 257–265, https://doi.org/10.1006/bbrc.1994.1697.
[60] C.C. Miller, V.A. Ziboh, Induction of epidermal hyperproliferation by topical n-3 polyunsaturated fatty acids on guinea pig skin linked to decreased levels of 13-hydroxyoctadecadienoic acid (13-hode), J. Invest Dermatol. 94 (1990) 353–358, https://doi.org/10.1111/1523-1747.ep12874482.
[61] Z. Naeem, S. Zukunft, S. Günther, S. Liebner, A. Weigert, B.D. Hammock, T. Frömel, I. Fleming, Role of the soluble epoxide hydrolase in the hair follicle stem cell homeostasis and hair growth, Pflug. Arch. Eur. J. Physiol. 474 (2022) 1021–1035, https://doi.org/10.1007/s00424-022-02709-4.
[62] R. Kesavan, T. Frömel, S. Zukunft, B. Brüne, A. Weigert, I. Wittig, R. Popp, I. Fleming, The consequences of soluble epoxide hydrolase deletion on tumorigenesis and metastasis in a mouse model of breast cancer, Int J. Mol. Sci. 22 (2021), https://doi.org/10.3390/ijms22137120.
[63] D. Jonnalagadda, D. Wan, J. Chun, B.D. Hammock, Y. Kihara, A soluble epoxide hydrolase Inhibitor, 1-trifluoromethoxyphenyl-3-(1-propionylpiperidin-4-yl) urea, ameliorates experimental autoimmune encephalomyelitis, Int. J. Mol. Sci. 22 (2021), https://doi.org/10.3390/ijms22094650.
[64] O. Jung, F. Jansen, A. Mieth, E. Barbosa-Sicard, R.U. Pliquett, A. Babelova, C. Morisseau, S.H. Hwang, C. Tsai, B.D. Hammock, L. Schaefer, G. Geisslinger, K. Amann, R.P. Brandes, Inhibition of the soluble epoxide hydrolase promotes albuminuria in mice with progressive renal disease, PLoS ONE 5 (2010) e11979, https://doi.org/10.1371/journal.pone.0011979.
[65] K. Meirer, D. Glatzel, S. Kretschmer, S.K. Wittmann, M. Hartmann, R. Blöcher, C. Angioni, G. Geisslinger, D. Steinhilber, B. Hofmann, R. Fürst, E. Proschak, Design, synthesis and cellular characterization of a dual inhibitor of 5-lipoxygenase and soluble epoxide hydrolase, Molecules 22 (2016), https://doi.org/10.3390/molecules22010045.
[66] B. Nandha, S.A. Ramareddy, H. Kuntal, Synthesis of substituted fluorobenzimidazoles as inhibitors of 5-lipoxygenase and soluble epoxide hydrolase for anti-inflammatory activity, Arch. Pharm. 351 (2018) e1800030, https://doi.org/10.1002/ardp.201800030.
[67] K. Hiesinger, J.S. Kramer, S. Beyer, T. Eckes, S. Brunst, C. Flauaus, S.K. Wittmann, L. Weizel, A. Kaiser, S.B.M. Kretschmer, S. George, C. Angioni, J. Heering, G. Geisslinger, M. Schubert-Zsilavecz, A. Schmidtko, D. Pogoryelov, J. Pfeilschifter, B. Hofmann, D. Steinhilber, S. Schwalm, E. Proschak, Design, synthesis, and structure-activity relationship studies of dual inhibitors of soluble epoxide hydrolase and 5-lipoxygenase, J. Med. Chem. 63 (2020) 11498–11521, https://doi.org/10.1021/acs.jmedchem.0c00561.
[68] U. Garscha, E. Romp, S. Pace, A. Rossi, V. Temml, D. Schuster, S. König, J. Gerstmeier, S. Liening, M. Werner, H. Atze, S. Wittmann, C. Weinigel, S. Rummler, G.K. Scriba, L. Sautebin, O. Werz, Pharmacological profile and efficiency in vivo of diflapolin, the first dual inhibitor of 5-lipoxygenase-activating protein and soluble epoxide hydrolase, Sci. Rep. 7 (2017) 9398, https://doi.org/10.1038/s41598-017-09795-w.
[69] A. Cronin, M. Decker, M. Arand, Mammalian soluble epoxide hydrolase is identical to liver hepoxilin hydrolase, J. Lipid Res 52 (2011) 712–719, https://doi.org/10.1194/jlr.M009639.
[70] M.B. Andberg, M. Hamberg, J.Z. Haeggström, Mutation of tyrosine 383 in leukotriene A4 hydrolase allows conversion of leukotriene A4 into 5S,6S-dihydroxy-7,9-trans-11,14-cis-eicosatetraenoic acid, Implic. epoxide hydrolase Mech., J. Biol. Chem. 272 (1997) 23057–23063, https://doi.org/10.1074/jbc.272.37.23057.
[71] A.V. Sorokin, A.F. Domenichiello, A.K. Dey, Z.-X. Yuan, A. Goyal, S.M. Rose, M. P. Playford, C.E. Ramsden, N.N. Mehta, Bioactive lipid mediator profiles in human psoriasis skin and blood, J. Invest Dermatol. 138 (2018) 1518–1528, https://doi.org/10.1016/j.jid.2018.02.003.
[72] D.M. Reilly, M.R. Green, Eicosanoid and cytokine levels in acute skin irritation in response to tape stripping and capsaicin, Acta Derm. Venereol. 79 (1999) 187–190, https://doi.org/10.1080/000155599750010931.
[73] H. Katayama, Development of psoriasis by continuous neutrophil infiltration into the epidermis, Exp. Dermatol. 27 (2018) 1084–1091, https://doi.org/10.1111/exd.13746.
[74] H.-C. Lin, T.-H. Lin, M.-Y. Wu, Y.-C. Chiu, C.-H. Tang, M.-J. Hour, H.-C. Liou, H.-J. Tu, R.-S. Yang, W.-M. Fu, 5-Lipoxygenase inhibitors attenuate TNF-α-induced inflammation in human synovial fibroblasts, PLoS ONE 9 (2014) e107890, https://doi.org/10.1371/journal.pone.0107890.
[75] D.A. Thompson, B.D. Hammock, Dihydroxyoctadecamonoenoate esters inhibit the neutrophil respiratory burst, J. Biosci. 32 (2007) 279–291, https://doi.org/10.1007/s12038-007-0028-x.
[76] K. Hildreth, S.D. Kodani, B.D. Hammock, L. Zhao, Cytochrome P450-derived linoleic acid metabolites EpOMEs and DiHOMEs: a review of recent studies, J. Nutr. Biochem 86 (2020) 108484, https://doi.org/10.1016/j.jnutbio.2020.108484.
[77] J. Hu, R. Popp, T. Frömel, M. Ehling, K. Awwad, R.H. Adams, H.-P. Hammes, I. Fleming, Müller glia cells regulate Notch signaling and retinal angiogenesis via the generation of 19,20-dihydroxydocosapentaenoic acid, J. Exp. Med 211 (2014) 281–295, https://doi.org/10.1084/jem.20131494.
[78] T.E. Rose, C. Morisseau, J.-Y. Liu, B. Inceoglu, P.D. Jones, J.R. Sanborn, B. D. Hammock, 1-Aryl-3-(1-acylpiperidin-4-yl)urea inhibitors of human and murine soluble epoxide hydrolase: structure-activity relationships, pharmacokinetics, and reduction of inflammatory pain, J. Med Chem. 53 (2010) 7067–7075, https://doi.org/10.1021/jm100691c.
[79] Y. Nakamura, T. Matsuzaka, S. Tahara-Hanaoka, K. Shibuya, H. Shimano, C. Nakahashi-Oda, A. Shibuya, Elovl6 regulates mechanical damage-induced keratinocyte death and skin inflammation, Cell Death Dis. 9 (2018) 1181, https://doi.org/10.1038/s41419-018-1226-1.
[80] M. Radu, J. Chernoff, An in vivo assay to test blood vessel permeability, J. Vis. Exp. (2013) e50062, https://doi.org/10.3791/50062.
[81] I. Fleming, B. Fisslthaler, M. Dixit, R. Busse, Role of PECAM-1 in the shear-stress-induced activation of Akt and the endothelial nitric oxide synthase (eNOS) in endothelial cells, J. Cell Sci. 118 (2005) 4103–4111, https://doi.org/10.1242/jcs.02541.
[82] Y. Han, J. Mora, A. Huard, P. Da Silva, S. Wiechmann, M. Putyrski, C. Schuster, E. Elwakeel, G. Lang, A. Scholz, T. Scholz, T. Schmid, N. de Bruin, P. Billuart, C. Sala, H. Burkhardt, M.J. Parnham, A. Ernst, B. Brüne, A. Weigert, IL-38 Ameliorates skin inflammation and limits IL-17 production from γδ T cells, 835-846.e5, Cell Rep. 27 (2019), https://doi.org/10.1016/j.celrep.2019.03.082.
[83] J. Ye, G. Coulouris, I. Zaretskaya, I. Cutcutache, S. Rozen, T.L. Madden, Primer-BLAST: a tool to design target-specific primers for polymerase chain reaction, BMC Bioinforma. 13 (2012) 134, https://doi.org/10.1186/1471-2105-13-134.
[84] S.H. Hwang, H.-J. Tsai, J.-Y. Liu, C. Morisseau, B.D. Hammock, Orally bioavailable potent soluble epoxide hydrolase inhibitors, J. Med Chem. 50 (2007) 3825–3840, https://doi.org/10.1021/jm070270t.
[85] T. Frömel, B. Jungblut, J. Hu, C. Trouvain, E. Barbosa-Sicard, R. Popp, S. Liebner, S. Dimmeler, B.D. Hammock, I. Fleming, Soluble epoxide hydrolase regulates hematopoietic progenitor cell function via generation of fatty acid diols, Proc. Natl. Acad. Sci. USA 109 (2012) 9995–10000, https://doi.org/10.1073/pnas.1206493109.
[86] R. Kesavan, T. Frömel, S. Zukunft, H. Laban, A. Geyer, Z. Naeem, J. Heidler, I. Wittig, E. Elwakeel, B. Brüne, A. Weigert, R. Popp, I. Fleming, Cyp2c44 regulates prostaglandin synthesis, lymphangiogenesis, and metastasis in a mouse model of breast cancer, Proc. Natl. Acad. Sci. USA 117 (2020) 5923–5930, https://doi.org/10.1073/pnas.1921381117.
[87] R. Abdel Malik, N. Zippel, T. Frömel, J. Heidler, S. Zukunft, B. Walzog, N. Ansari, F. Pampaloni, S. Wingert, M.A. Rieger, I. Wittig, B. Fisslthaler, I. Fleming, AMP-Activated protein kinase α2 in neutrophils regulates vascular repair via hypoxia-inducible factor-1α and a network of proteins affecting metabolism and apoptosis, Circ. Res. 120 (2017) 99–109, https://doi.org/10.1161/CIRCRESAHA.116.309937.